PFC/JA-91-13

Fast Electron Transport In Lower-Hybrid Current Drive

K. Kupfer and A. Bers

April 1991

Plasma Fusion Center
Massachusetts Institute of Technology
Cambridge, MA 02139 USA

This work was supported in part by National Science Foundation Grant No. ECS-88-22475 and in part by U.S. Department of Energy Grant No. DE-FG02-91ER-54109. Reproduction and disposal, in whole or part, by or for the United States government is permitted.

Submitted for publication in: *Physics of Fluids B: Plasma Physics*

FAST ELECTRON TRANSPORT IN LOWER-HYBRID CURRENT DRIVE

K. Kupfer and A. Bers

Fast Electron Transport In Lower-Hybrid Current Drive

K. Kupfer and A. Bers

Plasma Fusion Center and Research Laboratory of Electronics
Massachusetts Institute of Technology
Cambridge, Massachusetts 02139

Abstract

We generalize the quasilinear-Fokker-Planck formulation for lower-hybrid current drive to include the wave induced radial transport of fast electrons. Toroidal ray tracing shows that the wave fields in the plasma develop a large poloidal component associated with the upshift in $k_{\|}$ and the filling of the "spectral gap". These fields lead to an enhanced radial $E \times B$ drift of resonant electrons. Two types of radial flows are obtained: an outward convective flow driven by the asymmetry in the poloidal wave spectrum, and a diffusive flow proportional to the width of the poloidal spectrum. Simulations of Alcator C and JT60, show that the radial convection velocity has a broad maximum of nearly 1 m/sec and is independent of the amplitude of fields. In both cases, the radial diffusion is found to be highly localized near the magnetic axis. For JT60, the peak of the diffusion profile can be quite large, nearly 1 m^2/sec.

PACS Numbers: 52., 52.50.Gj, 52.25.Fi, 52.55.Fa

April 19, 1991

I Introduction

In steady state lower-hybrid current drive (LHCD), the toroidal current in tokamaks is sustained by fast electrons which absorb energy and momentum from externally injected waves. The dynamics of the fast electron population is well described by balancing wave induced quasilinear diffusion with collisional slowing down and pitch angle scattering off of fixed Maxwellian field particles. Here we consider a quasilinear-Fokker-Planck formulation which includes the wave induced radial transport of fast electrons, thus generalizing the radially local, velocity space treatments of LHCD [1,2,3].

Uehara [4] has suggested that the wave induced $E \times B$ drift leads to an inward pinch of resonant electrons during LHCD; recently this effect was incorporated in a phenomenological model to explain the scaling of the plasma confinement time with respect to auxilliary power and plasma current [5]. The wave induced radial flux of resonant electrons has also been considered by Meng-Fen and Wei-Min [6], where an ad hoc quasilinear model was devised on the basis of a limited numerical study of ray tracing results during single-pass absorption. A neoclassical treatment of wave induced current and transport has been given by Antonsen and Yoshioka [7] and is applicable to situations when the electron distribution is close to a Maxwellian. An important distinction of our work, is that we consider a detailed model of the wave fields which develop in the plasma under the relevant situation of multiple-pass absorption. Furthermore, we treat the case when the electron tail is a strong departure from a Maxwellian, as is typical in LHCD.

The best current drive efficiencies for LHCD experiments are achieved when the wave spectrum launched into the plasma is narrow and close to the accessibility limit [8,9,10], where accessibility refers to the minimum parallel index ($ck_{\|}/\omega$) which will penetrate to the interior of the plasma while remaining in the slow wave polarization [11]. For central electron temperatures up to a few keV, waves launched near the accessibility limit are very weakly damped and there results a significant "spectral gap" which must be filled before the waves can Landau damp on electrons. Because of the weak dissipation, the ray trajectories of the waves can make several toroidal transits and suffer numerous radial reflections. It has been shown that by including toroidal effects in the ray dynamics, the poloidal mode numbers of the rays can upshift [12] and thus fill the spectral gap [13]. The fields required to bridge the spectral gap thus have a significant poloidal component, which will contribute to the radial

$E \times B$ drift of resonant electrons. We use the previously developed ray-tracing model of Bonoli and Englade [13], to determine the fields inside the plasma, thereby allowing us to evaluate the radial flow of fast electrons.

The paper is organized as follows. The Fokker-Planck equation is discussed in Section II and a detailed derivation of the relevant quasilinear operator is given in Appendix A. In Section III, we derive a wave induced radial convection velocity and diffusion coefficient. The wave induced radial flux is discussed in Section IV. The method used to calculate the quasilinear diffusion coefficients by ray-tracing, including self-consistent resonant damping, is given in Section V. Our model is applied to both Alcator C and JT60 parameters, with the results presented in Sections VI and VII. In Section VIII, we discuss the results and give our conclusions.

II The Fokker-Planck Equation

Restricting the analysis to frequencies below the electron cyclotron frequency, allows us to consider the guiding center orbits of electrons, where the waves do not destroy the adiabatic invariance of the magnetic moment. During LHCD, trapped electrons absorb little of the wave energy, so we consider only well circulating electrons. (Trapped particle effects have been considered in [14,15] and can be important in electron-cyclotron, or fast wave current drive.) In the absence of the RF fields, the electron orbits are assumed to follow the magnetic field lines with a constant parallel velocity, u. We thus consider the evolution of the electron distribution function, $f(u, v_\perp, \rho, t)$, where $\frac{1}{2}v_\perp^2$ is the perpendicular energy and ρ is a radial variable which labels the magnetic flux surfaces. The evolution of f is given by

$$\frac{\partial}{\partial t} f = (\frac{\partial}{\partial t})_{ql} f + (\frac{\partial}{\partial t})_c f \quad , \tag{1}$$

which represents a balance between RF quasilinear diffusion and collisional pitch angle scattering and slowing down. Here, $(\partial/\partial t)_c$ is the linearized collision operator for electrons slowing down and pitch angle scattering in $(u, v_\perp)$ space, as given in various references (see e.g. [3]). The collisional contribution to radial transport has a negligible effect on the confinement of fast electrons and can be ignored; hence the collision operator does not act on the ρ dependence of f. The quasilinear operator (see Appendix A) is

$$(\frac{\partial}{\partial t})_{ql} f = \frac{1}{\mathcal{J}} \frac{\partial}{\partial \rho} \mathcal{J} [D_{\rho\rho} \frac{\partial}{\partial \rho} + D_{\rho u} \frac{\partial}{\partial u}] f + \frac{\partial}{\partial u} [D_{uu} \frac{\partial}{\partial u} + D_{u\rho} \frac{\partial}{\partial \rho}] f \quad . \tag{2}$$

Assuming that the RF fields remain in the slow wave (electrostatic) polarization, the quasilinear diffusion coefficients are:

$$\begin{aligned} D_{uu} &= \frac{\pi e^2}{2m_e^2} dV^{-1} \int^{dV} d^3x \sum_s |\Phi_s|^2 \delta(uk_\parallel^s - \omega)(k_\parallel^s)^2 \\ D_{\rho u} &= \frac{\pi e}{2m_e \bar{B}} dV^{-1} \int^{dV} d^3x \sum_s |\Phi_s|^2 \delta(uk_\parallel^s - \omega) k_\parallel^s k_p^s \\ D_{\rho\rho} &= \frac{\pi}{2\bar{B}^2} dV^{-1} \int^{dV} d^3x \frac{\bar{B}}{B} \sum_s |\Phi_s|^2 \delta(uk_\parallel^s - \omega)(k_p^s)^2 \quad , \end{aligned} \tag{3}$$

where $D_{u\rho} = D_{\rho u}$. Here $B = |\mathbf{B}(\mathbf{x})|$, where $\mathbf{B}$ is the equilibrium magnetic field. Also, $\mathcal{J}(\rho) = \bar{B} dV/d\rho$ and

$$\bar{B} = dV^{-1} \int^{dV} d^3x \, B(\mathbf{x}) \quad , \tag{4}$$

where the spatial integration is over the infinitesimal volume dV surrounding a flux surface, hence it represents a flux surface average. The RF scalar potential, $\Phi_{rf}(\mathbf{x}, t)$, is represented in eikonal form,

$$\Phi_{rf} = \frac{1}{2} \sum_s \Phi_s(\mathbf{x}) \exp i \left(\int^{\mathbf{x}} d\mathbf{x}' \cdot \mathbf{k}_s(\mathbf{x}') - \omega t \right) \quad + \text{c.c.} \quad , \tag{5}$$

where Φ_s and $\mathbf{k}_s$ are assumed to be slowly varying. The quantities $k_\parallel^s$ and k_p^s are defined as:

$$k_\parallel^s = \mathbf{k}_s \cdot \mathbf{b} \tag{6}$$

$$k_p^s = \mathbf{b} \times \mathbf{k}_s \cdot \nabla \rho \quad , \tag{7}$$

where $\mathbf{b}$ is the spatially varying unit vector along the equilibrium magnetic field. A detailed derivation of (2) is given in Appendix A.

For a small inverse aspect ratio tokamak with circular flux surfaces, we take $\rho = r + \Delta(r) \cos\theta$, where $\Delta(r)$ is the Shafranov shift [16]. In this case, we may take $dV = 4\pi^2 R_o \rho d\rho$, where R_o is the major radius. Furthermore, in the expressions for $D_{\rho u}$ and $D_{\rho\rho}$, we take $B \approx \bar{B} \approx B_o$, where the B_o is the toroidal field on axis. The basic physics of (2) is simple; resonant electrons experience a diffusion in u, due to the wave's parallel field, as well as a diffusion in ρ, due to the radial component of the $E_{rf} \times B$ drift. Because these two processes are coupled, the quasilinear operator also includes cross flows that are proportional to $D_{\rho u}$ and $D_{u\rho}$.

We simplify the problem of solving (1) by approximating the electron distribution function, f, as a fixed Maxwellian with respect to the perpendicular energy. In particular we assume

$$f = F(u,\rho,t)(2\pi v_e^2)^{-1}\exp(-v_\perp^2/2v_e^2) \quad , \tag{8}$$

where $v_e(\rho) = \sqrt{kT_e(\rho)/m_e}$. This approximation ignores the enhancement of the perpendicular energy due to the pitch angle scattering of resonant electrons with large parallel energy [2,3]. The main effect of the fully consistent perpendicular dynamics is to increase the current drive efficiency [3,17], since collisional losses to the bulk plasma are reduced at higher energies. Substituting (8) into (1) and integrating over the perpendicular energy yields the following equation for the evolution of $F(u,\rho,t)$:

$$\begin{aligned}\frac{\partial}{\partial t}F(u,\rho,t) &= \frac{1}{\rho}\frac{\partial}{\partial\rho}\rho[D_{\rho\rho}\frac{\partial}{\partial\rho} + D_{\rho u}\frac{\partial}{\partial u}]F \\ &\quad + \frac{\partial}{\partial u}[(D_{uu}+D_c)\frac{\partial}{\partial u} + D_c\frac{u}{v_e^2} + D_{u\rho}\frac{\partial}{\partial\rho}]F \quad ,\end{aligned} \tag{9}$$

where

$$D_c = (Z_i+2)\nu_o v_e^5/u^3 \quad , \tag{10}$$

$$\nu_o = \omega_{pe}^4 \ln\Lambda/(4\pi n_e v_e^3) \quad , \tag{11}$$

and Z_i is the ion charge state.

In the usual treatment of LHCD [1,2], it is assumed that the electron distribution function is established on a fast time scale by the RF diffusion in u seeking a radially local balance with collisional pitch angle scattering and slowing down. The radially local, one-dimensional Fokker-Planck equation is

$$\frac{\partial}{\partial t}F(u,\rho,t) = \frac{\partial}{\partial u}[(D_{uu}+D_c)\frac{\partial}{\partial u} + D_c\frac{u}{v_e^2}]F(u,\rho,t) \quad , \tag{12}$$

which has the steady state solution

$$F(u,\rho) = N\exp\left(\int^u \frac{-D_c u du}{v_e^2(D_c+D_{uu})}\right) \quad , \tag{13}$$

where N is determined by normalizing F. Since there are relatively few electrons in the tail, we may take $N = n_e(\rho)/[v_e(\rho)\sqrt{2\pi}]$, where $n_e(\rho)$ is the local electron density. With F given by (13), it follows that the local RF power absorbed by the resonant electrons,

$$S_{rf}(\rho) = -m_e\int du\, uD_{uu}\frac{\partial}{\partial u}F(u,\rho) \quad , \tag{14}$$

is completely dissipated by collisions with the bulk plasma. The local current density driven by the RF is

$$J_{rf}(\rho) = e \int du\, uF(u,\rho) \quad . \tag{15}$$

III Radial Convection and Diffusion

The Fokker-Planck equation, (9), is complicated by the presence of cross flows which come from the coefficients $D_{\rho u}$ and $D_{u\rho}$. It is possible to introduce a new "radial" coordinate, $x(u,\rho)$, such that (9) takes on the simplified form:

$$\begin{aligned} \frac{\partial}{\partial t}F(u,x,t) &= \frac{1}{J}\frac{\partial}{\partial x}J[D_x\frac{\partial}{\partial x} - V_x]F(u,x,t) \\ &\quad + \frac{1}{J}\frac{\partial}{\partial u}J[D_u\frac{\partial}{\partial u} - V_u]F(u,x,t) \quad , \end{aligned} \tag{16}$$

where

$$J = \rho\frac{\partial}{\partial x}\rho(u,x) \quad . \tag{17}$$

To find an expression for ρ, as well as for the coefficients D_x, V_x, D_u, and V_u, we transform (16) into the (u,ρ) coordinates and compare the result with (9). This yields the following:

$$D_u = D_{uu} + D_c \tag{18}$$

$$V_u = -D_c\frac{u}{v_e^2} \tag{19}$$

$$V_x\frac{\partial}{\partial x}\rho(u,x) = \frac{uD_cD_{\rho u}}{v_e^2(D_{uu}+D_c)} \tag{20}$$

$$D_x[\frac{\partial}{\partial x}\rho(u,x)]^2 = D_{\rho\rho} - \frac{D_{\rho u}^2}{D_{uu}+D_c} \tag{21}$$

$$\frac{\partial}{\partial u}\rho(u,x) = \frac{D_{\rho u}}{D_{uu}+D_c} \quad . \tag{22}$$

Equation (22) can be integrated by the method of characteristics,

$$\frac{d\rho'}{du'} = A(u',\rho') \quad , \tag{23}$$

where $A(u,\rho) \equiv D_{\rho u}/(D_{uu}+D_c)$. By integrating (23), subject to the initial condition $\rho'(0) = x$, one obtains $\rho = \rho'(u)$. We note that $A(u,\rho)$ is a non-singular function that is finite only in the resonant region of velocity space. Let us consider the relevant case, when the resonant region is limited to the interval $u_1 < u < u_2$, where u_1 and u_2 can be functions of ρ. Since $A(u,\rho)$ vanishes outside this interval, it follows from (23) that $\rho = x$

for $u < u_1$. Integrating (23) beyond u_1 leads to a displacement between ρ and x. Again, because $A(u,\rho)$ vanishes outside of the resonant region, $\rho = \rho'(u_2)$ for $u > u_2$. Defining $\Delta\rho(u,x) = \rho(u,x) - x$, one sees that $\Delta\rho$ will typically be small compared to the length scale of the radial variation of F, i.e. $|\Delta\rho\partial F/\partial\rho| \ll 1$, where $|\Delta\rho| \sim (u_2 - u_1)|D_{\rho u}|/(D_{uu} + D_c)$. This is because of the relative slowness of the radial diffusion in comparison to the diffusion in u. Hence we may take $\partial\rho/\partial x \approx 1$, in (17), (20), and (21).

Equation (16) allows for some straight forward physical interpretation. First, consider the collisionless diffusion of electrons between u_1 and u_2 (i.e. take $D_c = 0$, so that $V_u = V_x = 0$). Since the diffusion in u takes place on a faster time scale than the diffusion in x, the distribution function is flattened in u at fixed x. An electron diffusing between u_1 and u_2 at fixed x, is actually following the diffusion path $\rho = x + \Delta\rho(u,x)$. The fast diffusion in u appears as an incoherent oscillation in ρ about a slowly varying average, which is x. We may thus think of x as the "oscillation center". On the slow time scale, the "oscillation center" diffuses, due to the action of D_x. Now introduce the collisional drag, so that electrons are slowed down in u, at a rate of V_u. The effect of this on the radial motion, is to induce a slow drift of the "oscillation center", at a rate of V_x. When D_{uu} is large enough that a typical resonant electron can diffuse back and forth between u_1 and u_2, before being slowed down below u_1, then we may average D_x and V_x with respect to u, for $u_1 < u < u_2$. Hence, we obtain an average radial diffusion and convection of resonant electrons.

IV The Radial Flux

In this section, we make the connection between the radial convection and diffusion of Section (III) and the usual radial flux, which is obtained by integrating (9) over u. Using Γ_{rf} to denote the RF induced radial flux, one finds from (9) that

$$\Gamma_{rf} = -\int du[D_{\rho\rho}\frac{\partial}{\partial\rho} + D_{\rho u}\frac{\partial}{\partial u}]F(u,\rho) \quad . \tag{24}$$

Following the usual approach to transport theory, we may assume that $F = F_o + \epsilon F_1 + \epsilon^2 F_2 + ...$, where ϵ is a small parameter characterizing the slow radial evolution of (9) relative to the fast velocity space evolution. The RF Fokker-Planck elements are assumed to obey the relative ordering $D_{\rho\rho} \sim \epsilon D_{\rho u} \sim \epsilon^2 D_{uu}$. Balancing the zeroth order terms in (9) yields (13)

as an equation for $F_o(u,\rho)$. The radial flux in (24) can now be expressed as

$$\Gamma_{rf} = \int du[V_\rho F_o - (D_{\rho\rho}\frac{\partial F_o}{\partial \rho} + \epsilon D_{\rho u}\frac{\partial F_1}{\partial u})] \quad , \tag{25}$$

where

$$V_\rho(u,\rho) = \frac{uD_cD_{\rho u}}{v_e^2(D_c + D_{uu})} \quad . \tag{26}$$

To consistently determine the radial flux through second order in ϵ, we must obtain ϵF_1 as driven by the first order velocity space flux $D_{u\rho}\partial F_o/\partial\rho$. The first order equation is

$$[(D_{uu} + D_c)\frac{\partial}{\partial u} + \frac{D_c v_e^2}{u}]\epsilon F_1 = -D_{u\rho}\frac{\partial}{\partial \rho}F_o(u,\rho) \quad , \tag{27}$$

which is easily solved by the use of an integrating factor. Let us assume that in the resonant region the RF diffusion in u is dominant over the collisional drag, then (27) reduces to

$$\epsilon\frac{\partial}{\partial u}F_1 \approx \frac{-D_{u\rho}}{D_{uu} + D_c}\frac{\partial}{\partial \rho}F_o(u,\rho) \quad . \tag{28}$$

Substitution of (28) into (25), leads to the radial flux

$$\Gamma_{rf} = \int du(V_\rho F_o - D_\rho\frac{\partial F_o}{\partial \rho}) \quad , \tag{29}$$

where

$$D_\rho = D_{\rho\rho} - D_{\rho u}^2/(D_{uu} + D_c) \tag{30}$$

Comparing this with the results of Section (III), we integrate equation (16) over u. This leads to a flux in x which is nearly identical to (29). The differences are small because $\rho = x + \Delta\rho(u,x)$ and $\Delta\rho(u,x)$ is assumed to be of order ϵ, thus $V_\rho \approx V_x$ and $D_\rho \approx D_x$. Meng-Fen and Wei-Min [6] obtained a similar result to (29), except that they assumed an ad hoc relation between k_p and $k_\parallel$ in their definitions of $D_{\rho u}$ and $D_{\rho\rho}$. Furthermore, they did not obtain the second term in D_ρ (i.e. the one dependent on $D_{\rho u}$).

It is important to point out that an attempt to solve (9) by expanding F as a power series in ϵ, does not yield conventional transport equations. One finds that only the density moment of the second order equation will annihilate terms depending on F_2. Therefore, to obtain an equation for the energy flux one would have to solve an additional inhomogeneous equation for F_2. The underlying physical reason for this is that the RF delivers energy directly to the non-Maxwellian tail of F_o. The above expression for Γ_{rf} may yield only a small radial flux because of the relatively small population of resonant electrons. Of course this small population of electrons is important because it is very energetic and carries a

large plasma current. For example, the confinement properties of resonant electrons can be important in broadening the RF driven current profile [18] and reducing the current drive efficiency [19]; this is in spite of the fact that the total radial particle flux remains relatively small.

V Ray Tracing Calculation

We now discuss the ray-tracing calculation which determines the quasilinear diffusion coefficients inside the plasma. Following Bonoli and Englade [13], the wave vector is expressed as $\mathbf{k} = k_r \mathbf{e}_r + (m/r)\mathbf{e}_\theta + (n/R)\mathbf{e}_\phi$, where $R = R_o + r\cos\theta$. Here r and θ are ordinary polar coordinates and ϕ is the toroidal angle. The equilibrium magnetic field is given by a small inverse aspect ratio expansion including the Shafranov shift, so that $\mathbf{B} = B_r \mathbf{e}_r + B_\theta \mathbf{e}_\theta + B_\phi \mathbf{e}_\phi$. Using these expressions for $\mathbf{k}$ and $\mathbf{B}$, we find that

$$k_\parallel = [k_r B_r + (m/r)B_\theta + (n/R)B_\phi]/B \tag{31}$$

and

$$k_p = [\frac{k_r B_r}{B_p} + \frac{m B_\theta}{r B_p}]\frac{B_\phi}{B} - \frac{n B_p}{RB} \quad , \tag{32}$$

where $B_p^2 = B_\theta^2 + B_r^2$. The wave vectors inside the plasma are determined by ray tracing from some initial values at the plasma edge. The local dispersion relation is denoted as $D_o(\mathbf{x}, \mathbf{k}, \omega) = 0$, so that the ray equations are

$$\begin{aligned}
\dot{r} &= -\frac{\partial D_o/\partial k_r}{\partial D_o/\partial \omega} \\
\dot{\theta} &= -\frac{\partial D_o/\partial m}{\partial D_o/\partial \omega} \\
\dot{\phi} &= -\frac{\partial D_o/\partial n}{\partial D_o/\partial \omega} \\
\dot{k_r} &= \frac{\partial D_o/\partial r}{\partial D_o/\partial \omega} \\
\dot{m} &= \frac{\partial D_o/\partial \theta}{\partial D_o/\partial \omega} \\
\dot{n} &= \frac{\partial D_o/\partial \phi}{\partial D_o/\partial \omega} \quad .
\end{aligned} \tag{33}$$

To evolve the ray trajectories in time we use [13], where the dispersion relation includes electromagnetic and warm plasma effects and is given in Appendix B. The equilibrium is

axisymmetric so that n is conserved. The toroidal nature of the equilibrium makes $D_o(\mathbf{x},\mathbf{k},\omega)$ dependent on θ, so that m is not conserved. The initial edge values for $k_\parallel$ are chosen to represent the spectrum which couples into the plasma from the waveguide array. The initial edge values for m and θ are taken to be zero, where as r is chosen near the edge of the plasma towards the inside of the cut off layer. (Note, the edge value of k_r is determined by the dispersion relation.)

The quasilinear diffusion coefficients expressed in (3) are computed using the ray equations, where each ray is associated with some increment of the total RF power launched into the plasma. We assume that this increment of power, P_s, propagates along the s^{th} ray trajectory in a tube of cross-sectional area σ. The total propagating energy density inside the tube is $W_s = P_s/(\sigma v_s)$, where v_s is the group velocity (i.e. $v_s = |\dot{\mathbf{x}}|$ as given by the ray equations). Assuming that the rays which penetrate to the interior of the plasma remain in the slow wave polarization, W_s and $|\Phi_s|^2$ are related by

$$W_s = \frac{1}{4}\epsilon_o|\Phi_s|^2k^2\omega\frac{\partial}{\partial\omega}K(\mathbf{x},\mathbf{k},\omega) \quad , \tag{34}$$

where $K(\mathbf{x},\mathbf{k},\omega)$ is the permitivity function associated with the dispersion relation, as given in Appendix B. To simplify the notation, it is implied that quantities depending on $\mathbf{k}$ and $\mathbf{x}$ are evaluated along the s^{th} ray trajectory. The quasilinear diffusion coefficients are expressible as the sum of individual contributions from each of the rays. For example, D_{uu} in (3) is expressed as the the sum of incremental contributions ΔD_{uu}, where

$$\Delta D_{uu} = \frac{2\pi e^2}{\epsilon_o m_e^2}dV^{-1}\int^{dV}\frac{d^3x}{v_s\sigma}\frac{P_s}{(\omega\partial K/\partial\omega)}(\frac{k_\parallel}{k})^2\delta(uk_\parallel-\omega) \quad . \tag{35}$$

Writing $v_s = dl/dt$, where dl is the infinitesimal pathlength along the ray trajectory, the integral over the volume dV is easily done by assuming that the power is constant inside the cross sectional area σ, outside of which it vanishes. Hence σ cancels out of the calculation.

We now assume that the volume, dV, is finite and that the ray enters this volume at $t = t_o$ and leaves at $t = t_o + \Delta t$. It is easily seen that the contribution to D_{uu} is simply

$$\Delta D_{uu} = \frac{2\pi e^2}{\epsilon_o m_e^2}dV^{-1}\int_{t_o}^{t_o+\Delta t}\frac{dtP_s}{(\omega\partial K/\partial\omega)}(\frac{k_\parallel}{k})^2\delta(uk_\parallel-\omega) \quad . \tag{36}$$

The final expression for D_{uu} is obtained by summing over all the individual contributions, ΔD_{uu}, made by each ray on each transit through the volume dV. In a completely analagous

way, the incremental contributions to $D_{\rho u}$ and $D_{\rho\rho}$ are

$$\begin{aligned}\Delta D_{\rho u} &= \frac{2\pi e}{\epsilon_o m_e B_o} dV^{-1} \int_{t_o}^{t_o+\Delta t} \frac{dt P_s}{(\omega \partial K/\partial\omega)} (\frac{k_p k_\parallel}{k^2}) \delta(u k_\parallel - \omega) \\ \Delta D_{\rho\rho} &= \frac{2\pi}{\epsilon_o B_o^2} dV^{-1} \int_{t_o}^{t_o+\Delta t} \frac{dt P_s}{(\omega \partial K/\partial\omega)} (\frac{k_p}{k})^2 \delta(u k_\parallel - \omega) \quad . \end{aligned} \tag{37}$$

The power associated with each ray, P_s, is damped as the ray propagates into the plasma. In particular, $P_s(t)$ is determined along each ray according to $dP_s/dt = -2(\gamma_e + \gamma_c)P_s$, where γ_e is electron Landau damping and γ_c is collisional (non-resonant) damping. The collisional damping is relatively weak, except in the cooler plasma near the edge. The electron Landau damping is given by

$$\gamma_e = -\frac{\pi\omega_{pe}^2}{k^2(\partial K/\partial\omega)} n_e^{-1} \frac{\partial F}{\partial u} \quad , \tag{38}$$

where $F(u,\rho)$ is determined by (13). To start the calculation, we assume that F in (38) is Maxwellian. An ensemble of rays are launched at the edge of the plasma with specified initial values of P_s. The ray trajectories are calculated until each value of P_s has damped to approximately one percent of its initial value. During this time, D_{uu} is computed by summing up the increments ΔD_{uu} given by equation (36). When the rays have damped, $F(u,\rho)$ is re-computed from (13), which changes the damping according to (38). The rays are re-initialized and the procedure is iterated until consecutive calculations of D_{uu} are in good agreement. Generally, convergence is obtained in the least number of iterations by starting with relatively low input power, so that the first few iterates are not strong departures from a Maxwellian. Gradually the power is brought up to its full value and several more iterations are needed to obtain good results. An important self-consistency check is to calculate the power dissipated according to the integral

$$P_{rf} = 4\pi^2 R_o \int \rho d\rho \, S_{rf}(\rho) \quad , \tag{39}$$

where $S_{rf}(\rho)$ is determined by (14). This should agree with the total power which is electron Landau damped as calculated directly from following the evolution of P_s along each of the rays. The total RF driven current, I_{rf}, is determined by integrating the current density calculated directly from (15). Convergence is assumed when consecutive values of P_{rf} and I_{rf} are in agreement; we used the criteria that on consecutive iterations, P_{rf} and I_{rf} should change by less than 10 percent, with no increasing or decreasing trends. In addition to D_{uu}, we also calculate $D_{\rho u}$ and $D_{\rho\rho}$ by using (37). The radial convection velocity, V_ρ, and diffusion coefficient, D_ρ, are then obtained from (26) and (30).

The power spectrum which couples into the plasma from the waveguide array, can effectively be represented by

$$S(n_{\|}) = \begin{cases} S_a & \text{if } n_a < n_{\|} < n_b \\ S_b & \text{if } n_b < n_{\|} < n_c \\ 0 & \text{otherwise} \end{cases} , \tag{40}$$

where $n_{\|} \equiv ck_{\|}/\omega$. The total RF power injected is $P_{in} = S_a(n_a - n_b) + S_b(n_c - n_b)$. Consider a ray launched at the edge with an initial power of $P_s(0)$, at a parallel index of $n_{\|o}$; we take $P_s(0) = S(n_{\|o})(\Delta n_{\|})_s$, where $(\Delta n_{\|})_s$ is a small increment of $n_{\|}$ associated with the s^{th} ray, so that $P_{in} = \sum_s P_s(0)$. A large portion of the total RF power is launched in a relatively narrow spectral band between n_a and n_b, i.e. $(n_b - n_a)S_a \gg (n_c - n_b)S_b$ and $(n_b - n_a) \ll (n_c - n_b)$. Typically, n_a is close to the critical value of $n_{\|}$ for wave accessibility. A "spectral gap" occurs when n_b is too small for electron Landau damping to be effective, i.e. $n_b \lesssim c/4v_e$. Rays launched in this part of the spectrum can make many passes through the plasma during which time $k_{\|}$ is altered from its initial value due to large shifts in m. When $k_{\|}$ upshifts sufficiently, the rays will Landau damp, quasilinearly forming the electron tail.

The distribution function, $F(u,\rho)$, and the quasilinear diffusion coefficient, $D_{uu}(u,\rho)$, are represented numerically on a velocity space grid at each of 40 flux surfaces throughout the plasma. The grid points in u are spaced by an amount δu, where $\delta u = u^2 \delta n_{\|}/c$ and $\delta n_{\|}$ is fixed. Because of the sensitivity of $F(u,\rho)$ to the value of $D_{uu}(u,\rho)$ at low velocities, to obtain good results we had to make $\delta u/v_e \lesssim 10^{-2}$ at $u \sim 4v_e$. Because the corresponding $\delta n_{\|}$ is so small (typically less than 10^{-2}), many rays had to be launched into the plasma in order to prevent D_{uu} from having gaps between grid points. To obtain the results presented in Sections VI and VII, we launched 100 rays between n_a and n_b and an additional 150 between n_b and n_c; each ray was followed numerically until $P_s(t)$ was damped to less than one percent of its initial value.

VI Numerical Results - Alcator C

Let us consider the Alcator C experiment, which was previously simulated by Bonoli and Englade [13]. The parameters are $n_{eo} = 7.5 \times 10^{13}$ cm^{-3}, $T_{eo} = 1.5$ keV, $T_{io} = 0.7$ keV, $a = 16.5$ cm, $R_o = 64$ cm, $I_p = 170$ kA, and $B_o = 10$T. Here n_{eo}, T_{eo}, and T_{io} are the peak values of the electron density, electron temperature, and ion temperature, I_p is the toroidal

plasma current, and a is the minor radius of the plasma. The assumed profiles are described in Appendix C. The RF frequency is 4.6 GHz (i.e. $\omega/2\pi$). The Brambilla power spectrum is modeled by (40), where $n_a = 1.25$, $n_b = 2.0$, and $n_c = 7.0$; S_a and S_b are determined so that 70 percent of P_{in} is launched between n_a and n_b. (Note, we have ignored any power which couples into the plasma at negative $n_\parallel$.) For $P_{in} = 440\,\mathrm{kW}$, we found that the total power resonantly absorbed by electrons was $P_{rf} = 390\,\mathrm{kW}$, with the remaining 50 kW being damped non-resonantly through electron-ion collisions in the plasma periphery.

It is convenient to introduce the normalized diffusion coefficient,

$$\tilde{D}(u,\rho) = \frac{D_{uu}}{\nu_o v_e^2} \quad , \tag{41}$$

where D_{uu} is determined by the method described in Section V. For the Alcator C parameters given above, $\tilde{D}(u,\rho)$ is shown in Figure 1(a) at a flux surface in the plasma core ($\rho/a = .16$). The normalized diffusion coefficient is non-zero in the interval, $u_1 < u < u_2$, where $u_1 \sim 4v_e$ and $u_2 \sim c/n_a$. From (13) it is easy to see that when $\tilde{D} \gg (u_2 - u_1)v_e/u_1^2$, the electron distribution will be nearly flat in the resonant region. The tail of the electron distribution function is easily visualized by subtracting the bulk Maxwellian from the total distribution function. We define

$$F_T(u,\rho) = \frac{v_e}{n_e}F(u,\rho) - \frac{1}{\sqrt{2\pi}}\exp(-u^2/2v_e^2) \quad , \tag{42}$$

where F is given by (13). Figure 1(b) shows $F_T(u,\rho)$ as a function of u. We see that F_T rises rapidly to its maximum value near u_1 and then has a gentle negative slope until u approaches u_2, at which point the distribution function is rapidly depleted. In this case, the electron distribution is insensitive to the large fluctuations in the RF diffusion coefficient throughout most of the resonant region, because $\tilde{D}$ remains above a threshold value, which is typically about 3 [3]. However, the height of F_T is quite sensitive to the value of $\tilde{D}$ in the vicinity of u_1, where the upshifts are important in determining the spectrum. The effect of calculating D_{uu} with the self-consistent quasilinear damping, (38), is to enhance D_{uu} for velocities near u_1, resulting in a substantial increase in the height of F_T. Close to u_1 the self-consistent damping is decreased from that of the initial Maxwellian, because the slope of the distribution function is decreased by the RF diffusion. At larger values of u the Maxwellian damping rapidly decreases to zero, while the self-consistent damping remains relatively constant throughout the resonant region. The later effect tends to makes the non-self-consistent D_{uu} too peaked at high velocities where the rays experience little dissipation.

The radial profiles of the absorbed RF power density and RF driven current density, defined by (14) and (15), are shown in Figure 2. The integrated RF driven current for the above case was $I_{rf} = 90$ kA. As pointed out in the previous section, the current drive efficiency is enhanced when the collisional $v_\perp$ dynamics of the resonant electrons is properly included. By comparing the efficiency of our one-dimensional model to that obtained from numerical solutions of the two-dimensional Fokker-Planck equation [3,17], we expect that the current would be enhanced by a factor of 2 to 3. In fact, this is consistent with the results of Bonoli and Englade [13], who report that for nearly the same absorbed power, I_{rf} increases from 70 kA to 170 kA when the enhanced perpendicular energy of the resonant electrons is taken into account. To represent a steady-state situation in which all of the plasma current is driven by the RF, we want to inject enough power to make $I_{rf} = I_p$. However, because of the reduced efficiency obtained with the one dimensional model, we only injected enough power to bring I_{rf} within a factor of 2 of the required plasma current, otherwise we would be overestimating the required P_{in}.

Figure 3 shows V_ρ as a function of u at two flux surfaces in the plasma. We see that V_ρ is large and positive (radially outward) for u near u_1 and it becomes negative for u near u_2. For the upshifted part of the spectrum, the convection velocity will always be radially outward. This can easily be seen by considering the relevant physics. The dynamics of the resonant wave-particle interaction results in a correlation between the radial $E \times B$ drift, which is proportional to k_p, and the parallel acceleration, which is proportional to $k_\parallel$. Assuming that m is upshifted, then an outward radial drift occurs when electrons are accelerated by the waves to higher u. (Likewise, the radial drift is inward when electrons are slowed down by the waves.) On average, the waves accelerate electrons to higher u and the momentum gained from the waves is destroyed by collisions. Since the upshifted spectrum accumulates at lower phase velocities, V_ρ tends to be positive in this region. In addition to the upshifted spectrum, there will also be a component of the spectrum with m's that have shifted in the negative direction. In this case, when electrons are resonantly accelerated by the waves, the radial convection is inward. Since this part of the spectrum tends to accumulate near the accessibility limit, V_ρ will become negative for u near u_2.

Based on this physical picture, it is possible to derive a simple expression for $V_\rho(u,\rho)$. Since $D_{uu} \gg D_c$ for $u_1 < u < u_2$, we find from (26) that

$$V_\rho \approx \frac{uD_c}{v_e^2} \frac{D_{\rho u}}{D_{uu}} \quad . \tag{43}$$

Thus the convection velocity depends on the details of the wave spectrum through the ratio $D_{\rho u}/D_{uu}$, which is independent of the overall amplitude of the fields. We define the following average:

$$\langle A \rangle \equiv \frac{\int^{dV} d^3x \sum_s |\Phi_s|^2 \delta(uk_{\|} - \omega) A(\mathbf{k},\mathbf{x})}{\int^{dV} d^3x \sum_s |\Phi_s|^2 \delta(uk_{\|} - \omega)} \quad , \tag{44}$$

which is a weighted average of all the resonant contributions to $A(\mathbf{k},\mathbf{x})$ on a given flux surface (A is arbitrary). Using this average and the definitions of $D_{\rho u}$ and D_{uu} in (3), we may rewrite (43) as

$$V_\rho = \frac{u^2 D_c}{v_e^2 \omega_{ce} \omega} \langle k_p \rangle \quad , \tag{45}$$

where $\omega_{ce} = eB_o/m_e$. From (31) and (32) it follows that $k_{\|} \approx (n + m/q)/R_o$ and $k_p \approx m/r$, where we are assuming that the dominant contribution to k_p occurs when m is large (i.e. $|m|$ can be of order n). Here we ignore terms of order r/R_o, so that there is no distinction made between ρ and r. Since n is conserved and the initial edge value of m is taken to be zero, one finds that $k_{\|o} \approx n/R_o$ and $m \approx (k_{\|} - k_{\|o}) R_o q$, where $k_{\|o}$ is the initial edge value of $k_{\|}$. Thus one obtains the expression

$$k_p \approx (k_{\|} - k_{\|o}) \frac{R_o q}{r} \quad . \tag{46}$$

Substituting (46) into (45), we find that

$$V_\rho = (2 + Z_i) \frac{\nu_o v_e R_o q}{\omega_{ce} r} \left(\frac{v_e}{u}\right)^2 \left[1 - \frac{u}{c} \langle n_{\|o} \rangle\right] \quad , \tag{47}$$

where we have used the identity $\langle n_{\|} \rangle = c/u$. According to (44), $\langle n_{\|o} \rangle$ is a function of u and ρ, whose precise calculation depends on the details of the ray trajectory. However, because the power spectrum of the source, $S(n_{\|})$, is narrow compared to the spectrum which is found inside the plasma from the ray tracing, we may take $\langle n_{\|o} \rangle$ to be a constant. The prediction of (47) is shown in Figure 3 as a dotted line, where have taken $\langle n_{\|o} \rangle \approx n_b = 2.0$. Thus, we see that the k_p spectrum inside the plasma develops an asymmetry due to upshifts in the m values of the rays. This asymmetry contributes to V_ρ, which can be estimated reasonably well by treating $\langle n_{\|o} \rangle$ as a constant in (47).

The average defined in (44) may be used to obtain an expression relating D_ρ to D_{uu}. Since $D_{uu} \gg D_c$ it follows from (30) that

$$D_\rho \approx D_{\rho\rho} - D_{\rho u}^2 / D_{uu} \quad . \tag{48}$$

Using the definitions of D_{uu}, $D_{\rho u}$, and $D_{\rho\rho}$, we may rewrite (48) as

$$D_\rho = D_{uu}(\frac{u}{\omega_{ce}\omega})^2(\langle k_p^2\rangle - \langle k_p\rangle^2) \quad . \tag{49}$$

Thus D_ρ depends on the spectral width, $(\langle k_p^2\rangle - \langle k_p\rangle^2)$. Figure 4(a) shows $D_\rho(u,\rho)$ at a flux surface in the core of the plasma and Figure 4(b) shows $D_{\rho\rho}$ at the same flux surface. We see that D_ρ is significantly smaller than $D_{\rho\rho}$. This is because there is a large asymmetry in $\langle k_p\rangle$. Under such circumstances, it is important to include the effect of $D_{\rho u}$ in determining the overall radial diffusion.

Because D_{uu} is so large, electrons are diffused rapidly between u_1 and u_2. It is therefore appropriate to consider the following velocity averages of V_ρ and $D_{\rho\rho}$:

$$\bar{V}_\rho(\rho) = N_T^{-1}\int du V_\rho(u,\rho)F_T(u,\rho) \tag{50}$$

$$\bar{D}_\rho(\rho) = N_T^{-1}\int du D_\rho(u,\rho)F_T(u,\rho) \tag{51}$$

where $N_T(\rho) = \int du F_T(u,\rho)$. The quantities $\bar{V}_\rho(\rho)$ and $\bar{D}_\rho(\rho)$ are shown in Figures 5(a) and 5(b). We see that $\bar{V}_\rho(\rho)$ is positive over a broad region of the plasma. The radial diffusion coefficient, $\bar{D}_\rho(\rho)$, has a relatively narrow profile which is sharply peaked near the center.

VII Numerical Results - JT60

The parameters for the JT60 current drive experiments are [10]: $n_{eo} = 3.0\times10^{13}\,\mathrm{cm}^{-3}$, $T_{eo} = 3.0\,\mathrm{keV}$, $T_{io} = 3.0\,\mathrm{keV}$, $a = 70\,\mathrm{cm}$, $R_o = 310\,\mathrm{cm}$, $I_p = 1.5\,\mathrm{MA}$, and $B_o = 4.5\mathrm{T}$. The RF frequency is 2 GHz. The power spectrum of the multi-junction waveguide array is very narrow and is modeled by (40), where $n_a = 1.25$, $n_b = 1.75$, and $n_c = 4.75$; S_a and S_b are determined so that 80 percent of P_{in} is launched between n_a and n_b. For $P_{in} = 4.6\,\mathrm{MW}$, the total power resonantly absorbed by electrons was $P_{rf} = 4.2\,\mathrm{MW}$, the remainder being absorbed non-resonantly through collisions.

The normalized diffusion coefficient, $\tilde{D}$, defined in (41), is shown in Figure 6(a) at a flux surface in the core of the plasma ($\rho/a = .16$). As expected, $\tilde{D}$, is non-zero in the interval $u_1 < u < u_2$, where $u_1 \sim 4v_e$ and $u_2 \sim c/n_a$. The corresponding distribution function, F_T, defined in (42), is shown Figure 6(b). Comparing Figure 6 with Figure 1, we see that throughout most of the resonant region, $\tilde{D}$ is significantly larger for JT60 than for Alcator C, but the height of F_T is nearly the same in both cases. This is because F_T is not sensitive

to the value of $\tilde{D}$, except in a narrow region near u_1. (Because $\tilde{D}$ is so large, one might be concerned about trapping effects [20]. However, a brief calculation shows that for JT60 parameters $\tau_{ac}/\tau_{tr} \sim 10^{-2}$ [21].) Figure 7 shows the radial profiles of S_{rf} and J_{rf}; the integrated RF driven current is $I_{rf} = 730$ kA, which is a factor of 2 smaller than I_p.

The radial convection velocity, $V_\rho(u,\rho)$, is shown in Figure 8 at two flux surfaces in the plasma. The prediction of (47) is shown as a dotted line, where we have taken $\langle n_{\|o}\rangle \approx n_b = 1.75$. Comparing this to the Alcator results shown in Figure (3), it is seen that the JT60 results are predicted more closely by (47) at the low end of the phase velocity spectrum. We think that this is because the source spectrum $S(n_\|)$ is narrower, so that taking $\langle n_{\|o}\rangle$ to be a constant is a better approximation. The radial diffusion coefficient, $D_\rho(u,\rho)$, is shown in Figure 9(a) at fixed ρ. For comparison, Figure 9(b) shows the Fokker-Planck coefficient $D_{\rho\rho}(u,\rho)$. Again we see that there is a significant reduction in the radial diffusion due to the off-diagonal Fokker-Planck coefficients. Figure 10 shows the profiles of the average convection velocity and the average radial diffusion coefficient, defined by (50) and (51). The average convection velocity is positive throughout the core of the plasma, with a broad maximum at $\rho/a \approx 0.1$. The diffusion coefficient is highly peaked near the magnetic axis. This is because the poloidal component of the wavefield becomes large as the rays approach the central portion of the plasma. However, rays with finite m never actually pass through the magnetic axis, because this is disallowed by the ray equations (33), thus D_ρ vanishes on axis.

We may obtain further understanding of the RF induced radial diffusion by examining the relationship between D_ρ and D_{uu}. Substituting (46) into (49), we find

$$D_\rho = D_{uu}\left(\frac{R_o q}{r\omega_{ce}}\right)^2 \left[\sigma(u,\rho)\frac{u}{c}\right]^2 \quad , \tag{52}$$

where

$$\sigma(u,\rho) = [\langle n_{\|o}^2\rangle - \langle n_{\|o}\rangle^2]^{1/2} \quad . \tag{53}$$

Because the source spectrum is relatively narrow compared to the spectrum in the plasma, we may try approximating σ as a constant determined by the width of $S(n_\|)$. Of course, one must know D_{uu} in order for (52) to be useful. Using the results of the above JT60 simulation, we calculate D_ρ from (52), assuming that $\sigma \approx .3(n_b - n_a) = .15$. The result is shown in Figure 11(a), which should be compared to D_ρ obtained directly from the ray tracing, as shown in Figure 11(b). We see that with σ taken as a constant, the prediction of (52) only gives good agreement at the high end of the phase velocity spectrum. Using

this approximation for Alcator C yields worse results than for JT60; we believe this is due to Alcator's broader source spectrum.

We would like to comment on two aspects of the calculation. First, the power spectrum of the source, $S(n_\parallel)$, includes a low intensity, high $n_\parallel$ tail between n_b and n_c. The presence of this part of the spectrum is important in filling the spectral gap at intermediate radial positions, where the plasma is cooler and the electron damping is weaker. Figure 12 shows $\tilde{D}(u,\rho)$ and $F_T(u,\rho)$ at $\rho/a = 0.49$. We see that although $\tilde{D}$ is relatively small for u/v_e between 4 and 5.5, it is nonetheless effective in elevating a substantial value of F_T. When the high $n_\parallel$ part of the source is not included, then $\tilde{D}$ is too small at low phase velocities and F_T drops by orders of magnitude. The result is that the power deposition, $S_{rf}(\rho)$, becomes more concentrated near the center, where the local current drive efficiency is lower (the efficiency is inversely proportional to the density) and the total RF driven current is substantially reduced.

We would also like to comment on the role of self-consistency in determing the Fokker-Planck elements. We have already discussed how the self-consistent spectrum tends to be enhanced at lower phase velocities in comparison to that obtained with a fixed Maxwellian electron population. This result, however, has little effect on the convection velocity, since (47) holds whether the fields are self-consistent or not. The radial diffusion coefficient, as expressed in (49), is proportional to D_{uu} and will be affected by the details of spectrum inside the plasma. To make a direct comparison of the results, we examined the above JT60 case by doing the ray tracing part of the calculation on a fixed Maxwellian plasma, i.e. without iterating to obtain the self-consistent damping. Using the D_{uu} from this calculation, we then calculated $F(u,\rho)$ according to (13). The total RF driven current obtained from this distribution function was four times smaller than that obtained in the self-consistent calculation. The average convection velocity, $\bar{V}_\rho(\rho)$, changed very little. The profile of $\bar{D}_\rho(\rho)$, was somewhat broader in the non-self-consistent case, with the peak being reduced by less than a factor of 2.

VIII Conclusions and Discussion

We have extended the quasilinear-Fokker-Planck formulation of LHCD to include the wave induced radial transport of fast electrons, as given by (2). The dominant transport mecha-

nism is the $E_{rf} \times B$ drift that arises when the waves in the plasma have a significant poloidal component. The radial flux of resonant electrons is determined by the convection velocity V_ρ, defined in (26), and the diffusion coefficient D_ρ, defined in (30). The convection velocity depends on $\langle k_p \rangle$, as given in (45), where the averaging procedure is defined in (44) and requires knowledge of the fields inside the plasma. Similarly, D_ρ depends on $(\langle k_p^2 \rangle - \langle k_p \rangle^2)$, as given in (49). It is interesting to note that while D_ρ is proportional to Φ_{rf}^2, V_ρ tends to be independent of the amplitude of the fields. The radial convection depends on the amount of momentum absorbed from the waves and the ratio of $k_p/k_\parallel$ at resonance; since the momentum absorbed from the waves is balanced by the momentum destroyed in collisions with the bulk plasma, the radial convection is proportional to D_c and independent of the wave amplitude. There is generally a large asymmetry in $\langle k_p \rangle$, because toroidal effects on the wave propagation tend to fill in the spectral gap. This leads to a net outward radial convection, which can be well understood on the basis of (47). Toroidal wave propagation tends to significantly broaden the poloidal spectrum, leading to an enhancement in D_ρ, the scaling of which is easily seen in (52). These results, together with the results of our numerical simulations, given in Figures 5 and 10, are entirely new.

It is evident from our numerical results for Alcator C and JT60, that the wave induced radial convection velocity is outward, on average. This stands in direct contradiction with the inward pinch effect of Uehara [5]. Uehara assumes that the wave vector of the RF field inside the plasma maintains the relation $\mathbf{k} = k_\phi \mathbf{e}_\phi + k_r \mathbf{e}_r$. Making this assumption, it follows that $k_\parallel \approx k_\phi$ and $k_p \approx -k_\phi B_\theta / B$. Substituting these relations into (45), one finds that $V_\rho \approx -u D_c B_\theta / (v_e^2 \omega_{ce} B)$, which indeed corresponds to an inward flux of resonant electrons. This inward pinch cannot occur in LHCD, because as the waves propagate into the plasma toroidal effects drastically alter the direction of $\mathbf{k}$, so that it is not valid to ignore the poloidal component of the fields. (Evidently Uehara also ignores the self-consistent flattening of the electron distribution function across the resonant region, which occurs because $D_{ql} \gg D_c$. This effect substantially reduces V_ρ, so that it tends to be independent of the amplitude of the RF field.)

We now turn to a discussion of the physical results of our calculations. It is important to compare the RF induced radial diffusion and convection, with the effects of anomalous electron confinement. The anomalous confinement time of fast electrons is often assumed to have the form $\tau_l = \tau_o \gamma^p$, where τ_o is the empirical confinement time of the bulk electrons and $\gamma = (1 - v^2/c^2)^{-1/2}$. The factor γ^p appears as an enhancement of the confinement time

at high energies [22], which is in agreement with observations of runaway electrons. For Alcator C, $\tau_o \sim 5$ msec and $p \approx 3$, so that a typical resonant electron has $\eta \lesssim 10$ msec [13]. This confinement time corresponds to an anomalous radial diffusion process of roughly $1\text{m}^2/\text{sec}$. Hence, for Alcator C the wave induced radial diffusion, shown in Figure 5(b), is clearly dominated by anomalous diffusion and can thus have little effect on the dynamics of the fast electrons. On the other hand, the wave induced radial diffusion calculated for JT60, shown in Figure 10(b), is competitive with anomalous diffusion in a narrow radial shell near the magnetic axis. Because the radial extent of $\bar{D}_\rho$ is so narrow, we must conclude that anomalous diffusion is also the dominating effect on JT60. A crude way of judging the importance of the wave induced radial convection velocity is to compare it to anomalous diffusion acting over a gradient length scale of the order of the minor radius, i.e. radial convection is important when $\bar{V}_\rho \sim D_A/a$, where D_A is the anomalous diffusion coefficient. For both Alcator C and JT60 the radial profile of $\bar{V}_\rho$ is positive across most of the plasma and has a broad maximum of nearly 1 m/sec. Assuming $D_A \sim 1\text{m}^2/\text{sec}$, we see that the convection velocity on JT60 may be of consequence, where as on Alcator C it is more clearly dominated by anomalous diffusion. We note that studies done on Versator II, using an innovative cyclotron diagnostic, concluded no noticeable difference in the fast electron confinement time for LHCD when compared to inductive current drive [23]. Because of the short electron confinement time on Versator II, this result does not contradict our calculations of the expected wave induced diffusion and convection.

We would like to briefly comment on the validity of the ray-tracing calculation, which determines the spectrum inside the plasma. Inspection of the ray trajectories reveals that as the rays reflect near the center of the plasma, the variation of k_r becomes rapid, and the validity of geometric optics becomes questionable. Because the rays make many transits through the plasma, it may be more appropriate to consider a normal mode description of the RF fields [24,25]. It is likely that such considerations would lead to a modification of our results in a narrow region near the magnetic axis. This would be most important for the radial diffusion, since it is so highly peaked near the center.

Finally, we would like to comment on several aspects of the calculation that should be improved for future studies. The main deficiency of the calculation, is that we solve for $F(u,\rho)$ without self-consistently including the radial fluxes. In particular, we solve for the steady-state of (12), as opposed to (9). A steady state solution of (9) could be obtained by replacing the time derivative of F with a low energy electron source in the central portion

of the plasma, intended to compensate for the loss of fast electrons at the edge. One then solves (9) as an elliptic equation with the appropriate boundary conditions on the distribution function; numerical techniques based on this approach have been used successfully to solve for the radially local, electron distribution function in two-dimensional velocity space [26]. Using this approach, one could study the effect of anomalous radial diffusion, by simply adding D_A to $D_{\rho\rho}$ in (9). A remaining problem, regards the self-consistent $v_\perp$ dynamics, which leads to a well known enhancement of the perpendicular energy of resonant electrons. Without this effect, our current drive efficiency is too small by a factor of 2 to 3. Since it is computationally too expensive to solve for the three dimensional distribution function, $f(u, v_\perp, \rho)$, and self-consistently determine the Fokker-Planck elements from a ray-tracing calculation, a remaining problem is to find a way of reducing this to a two-dimensional model, while still retaining the effects of the fully consistent three-dimensional dynamics.

IX Acknowledgements

We wish to acknowledge fruitful discussions with Dr. Abhay Ram and Dr. Paul Bonoli. We also wish to thank Dr. Bonoli for the use of his ray tracing code. This work was supported in part by National Science Foundation Grant No. ECS-88-22475 and in part by United States Department of Energy Grant No. DE-FG02-91ER-54109.

Appendices

A Quasilinear Theory

To derive the quasilinear operator for LHCD, including radial diffusion, we proceed from the drift kinetic equation, using the guiding center theory of Littlejohn [27]. Our approach is quite similar to that used by Chiu [28]. The guiding center equations of motion for electrons are

$$\dot{\mathbf{x}} = u\frac{\mathbf{B}^\star}{\mathbf{B}^\star_\parallel} + \frac{\mathbf{b}}{\mathbf{B}^\star_\parallel} \times (\nabla\Phi_{rf} - \frac{m_e}{e}M\nabla B)] \quad , \tag{54}$$

$$\dot{u} = \frac{\mathbf{B}^\star}{B^\star_\parallel} \cdot (\frac{e}{m_e}\nabla\Phi_{rf} - M\nabla B) \quad , \tag{55}$$

where $\mathbf{B}^\star = \mathbf{B} - (m_e u/e)\nabla\times\mathbf{b}$ and $B^\star_\parallel = \mathbf{b}\cdot\mathbf{B}^\star$. (Note, that we use e to denote the magnitude of charge on an electron, i.e. it is positive.) Here M is the magnetic moment of an electron, and is an adiabatic invariant (to lowest order in the guiding center expansion $M = v_\perp^2/2B$). Also we have evaluated Φ_{rf} at the guiding center, so that $k_\perp v_\perp/\omega_{ce}$ is assumed to be small. The drift kinetic equation for the gyro-averaged electron distribution function is

$$[\frac{\partial}{\partial t} + \dot{\mathbf{x}}\cdot\nabla + \dot{u}\frac{\partial}{\partial u}]f(\mathbf{x}, u, M, t) = 0 \quad . \tag{56}$$

We now write

$$\begin{aligned} \dot{\mathbf{x}} &= \dot{\mathbf{x}}_o + \dot{\mathbf{x}}_1 \\ \dot{u} &= \dot{u}_o + \dot{u}_1 \quad , \end{aligned} \tag{57}$$

where $\dot{\mathbf{x}}_1$ is the term in (54) which is proportional to Φ_{rf} and $\dot{u}_1$ is defined in an analogous manner. Similarly, we write $f = f_o + f_1$, so that the linearized drift kinetic equation is

$$(\frac{d}{dt})_o f_1 = -(\dot{\mathbf{x}}_1\cdot\nabla + \dot{u}_1\frac{\partial}{\partial u})f_o \quad , \tag{58}$$

where

$$(\frac{d}{dt})_o = [\frac{\partial}{\partial t} + \dot{\mathbf{x}}_o\cdot\nabla + \dot{u}_o\frac{\partial}{\partial u}] \quad . \tag{59}$$

The quasilinear equation for f_o is

$$(\frac{d}{dt})_o f_o = -(B^\star_\parallel)^{-1}[\nabla\cdot\langle B^\star_\parallel\dot{\mathbf{x}}_1 f_1\rangle + \frac{\partial}{\partial u}\langle B^\star_\parallel\dot{u}_1 f_1\rangle] \quad , \tag{60}$$

where the angular brackets denote a coarse-graining in space at the scale of the RF wavelength, as well as a time average over the fast oscillation at the RF frequency. In deriving (60), we have used the identity

$$\nabla \cdot (B_\parallel^\star \dot{\mathbf{x}}_1) + \frac{\partial}{\partial u}(B_\parallel^\star \dot{u}_1) = 0 \quad , \tag{61}$$

which follows directly from (54) and (55).

With the wave fields expressed in eikonal form, as given by (5), the linear solution is obtained by writing f_1 in a similar fashion,

$$f_1 = \frac{1}{2}\sum_s f_s(\mathbf{x}, u, M) \exp i\left(\int^{\mathbf{x}} d\mathbf{x}' \cdot \mathbf{k}_s(\mathbf{x}') - \omega t\right) \quad + \text{c.c.} \quad . \tag{62}$$

Ignoring the slow variations in (58) one obtains the solution

$$f_s = -(\mathbf{k}_s \cdot \dot{\mathbf{x}}_o - \omega)^{-1} \Phi_s L_s f_o \quad , \tag{63}$$

where L_s is the operator

$$L_s = (B_\parallel^\star)^{-1}[\frac{e}{m_e}\mathbf{B}^\star \cdot \mathbf{k}_s \frac{\partial}{\partial u} + \mathbf{b} \times \mathbf{k}_s \cdot \nabla] \quad . \tag{64}$$

Using (63), one obtains

$$\langle B_\parallel^\star \dot{\mathbf{x}}_1 f_1 \rangle = -\frac{\pi}{2}\sum_s \mathbf{b} \times \mathbf{k}_s |\Phi_s|^2 \delta(\mathbf{k}_s \cdot \dot{\mathbf{x}}_o - \omega) L_s f_o \tag{65}$$

$$\langle B_\parallel^\star \dot{u}_1 f_1 \rangle = -\frac{\pi}{2}\sum_s \frac{e}{m_e}\mathbf{B}^\star \cdot \mathbf{k}_s |\Phi_s|^2 \delta(\mathbf{k}_s \cdot \dot{\mathbf{x}}_o - \omega) L_s f_o \quad , \tag{66}$$

as needed for the right side of (60).

The next step in the derivation of the quasilinear operator used in the text, is to recognize that (60) contains several time scales. We will ignore all terms involving the equilibrium perpendicular guiding center drifts, since these are only needed to obtain the neoclassical transport effects. Thus we take $\mathbf{B}^\star = \mathbf{B}$ and $\dot{\mathbf{x}}_o = u\mathbf{b}$, everywhere in (60). The operator on the left side of (60), is $(d/dt)_o = (\frac{\partial}{\partial t} + u\mathbf{b} \cdot \nabla)$, where we have ignored the small oscillations in u caused by the parallel magnetic gradient acting on well circulating electrons. Using the identity

$$dV^{-1}\int^{dV} d^3x\, \nabla \cdot \mathbf{A} = (\frac{dV}{d\rho})^{-1}\frac{\partial}{\partial \rho}[\frac{dV}{d\rho}\, dV^{-1}\int^{dV} d^3x\, (\mathbf{A} \cdot \nabla\rho)] \quad , \tag{67}$$

we multiply (60) by B and flux surface average. This annihilates the term $u\mathbf{b} \cdot \nabla f_o$, as well as several terms on the right side of (60). We write $f_o = \bar{f}_o + \delta f_o$, where $\bar{f}_o$ is the flux surface

average of f_o and δf_o is small because the parallel streaming smooths out any variations in the flux surface. Finally, we obtain

$$\begin{aligned}\frac{\partial}{\partial t}\bar{f}_o &= \frac{1}{\mathcal{J}}\frac{\partial}{\partial \rho}\mathcal{J}[D_{\rho\rho}\frac{\partial}{\partial \rho}+D_{\rho u}\frac{\partial}{\partial u}]\bar{f}_o \\ &\quad +\frac{\partial}{\partial u}[D_{uu}\frac{\partial}{\partial u}+D_{u\rho}\frac{\partial}{\partial \rho}]\bar{f}_o \quad . \end{aligned} \tag{68}$$

where $\mathcal{J}=\bar{B}dV/d\rho$ and the quasilinear diffusion coefficients are defined in (3). Note, the volume element in the reduced phase space is $2\pi\mathcal{J}dudMd\rho$. In the text we have dropped the bar and subscript on the average distribution function.

B The Dispersion Relation

The local dispersion relation for lower-hybrid waves includes electromagnetic and warm plasma effects [13]. The ions are taken to be unmagnetized and the electrons are treated as strongly magnetized, in the limit $(k_\perp\rho_e)^2 \ll 1$. The local dispersion relation is

$$D_o(\mathbf{x},\mathbf{k},\omega)=P_6n_\perp^6+P_4n_\perp^4+P_2n_\perp^2+P_o \tag{69}$$

where

$$\begin{aligned}P_o &= \epsilon_\parallel[(n_\parallel^2-\epsilon_\perp)^2-\epsilon_{xy}] \\ P_2 &= (\epsilon_\perp+\epsilon_\parallel)(n_\parallel^2-\epsilon_\perp)+\epsilon_{xy}^2 \\ P_4 &= \epsilon_\perp \\ P_6 &= -\left(3\frac{\omega_{pi}^2}{\omega^2}\frac{v_i^2}{c^2}+\frac{3}{4}\frac{\omega_{pe}^2}{\omega_{ce}^2}\frac{\omega^2}{\omega_{ce}^2}\frac{v_e^2}{c^2}\right) \quad . \end{aligned} \tag{70}$$

We are using the notation $n_\perp=ck_\perp/\omega$, $n_\parallel=ck_\parallel/\omega$, $k_\perp=|\mathbf{k}-k_\parallel\mathbf{B}/B|$, and $k_\parallel=\mathbf{k}\cdot\mathbf{B}/B$. Also $\epsilon_\perp$, $\epsilon_\parallel$, and ϵ_{xy} are the elements of the cold plasma dielectric tensor, where $\mathbf{B}=B\mathbf{e}_z$. They are given by

$$\begin{aligned}\epsilon_\perp &= 1+(\frac{\omega_{pe}}{\omega_{ce}})^2-(\frac{\omega_{pi}}{\omega})^2 \\ \epsilon_\parallel &= 1-(\frac{\omega_{pi}}{\omega})^2-(\frac{\omega_{pe}}{\omega})^2 \\ \epsilon_{xy} &= \frac{\omega_{pe}^2}{\omega_{ce}\omega} \quad . \end{aligned} \tag{71}$$

All plasma parameters are slowly varying functions of $\mathbf{x}$. The normalized effective permitivity function is

$$K(\mathbf{x},\mathbf{k},\omega)=D_o(\mathbf{x},\mathbf{k},\omega)/(n_\perp^2+n_\parallel^2)^2 \quad . \tag{72}$$

C The Profiles

In the Bonoli-Englade code [13], the plasma profiles are assumed to be of the following form:

$$\begin{aligned} n_e(\rho) &= (n_{eo} - n_{ea})\frac{\exp(\xi_n) - \exp(\xi_n \rho^2/a^2)}{\exp(\xi_n) - 1} + n_{ea} \\ T_e(\rho) &= (T_{eo} - T_{ea})\frac{\exp(-\xi_e \rho^2/a^2) - \exp(-\xi_e)}{1 - \exp(-\xi_e)} + T_{ea} \\ T_i(\rho) &= (T_{io} - T_{ia})\frac{\exp(-\xi_i \rho^2/a^2) - \exp(-\xi_i)}{1 - \exp(-\xi_i)} + T_{ia} \quad , \end{aligned} \tag{73}$$

where a is the radius of the limiter, and ρ is the radius of any given flux surface inside the plasma. Beyond the limiter, an ideally conducting chamber surrounds the plasma at $\rho = b$. The profiles are assumed to fall off linearly for $a \leq \rho \leq b$, where $T_e(b)$ and $T_i(b)$ are taken to be about 15 percent of their respective values at $\rho = a$. The q profile is assumed to be

$$q(\rho) = 1 + \xi_b(\rho/a)^2 \quad , \tag{74}$$

where ξ_b is determined by requiring $q(a) = 2\pi a^2 B_o/(R_o \mu_o I_p)$, since the current density vanishes for $\rho > a$. Here B_o is the magnetic field on axis, R_o is the major radius, and I_p is the total plasma current. The Shafranov inverse aspect ratio expansion is used to obtain $\mathbf{B}(r, \theta)$ and $\rho(r, \theta)$ [16]; explicit forms are given by Bonoli and Englade [13].

The profile factors for Alcator C were taken after Bonoli to be $\xi_e = 3.99$, $\xi_i = 3.29$, $\xi_n = -0.92$, $T_{ea} = T_{ia} = 0.03$ keV, and $n_{ea} = 1.1 \times 10^{13}$ cm^{-3}. For JT60, we chose $\xi_e = \xi_i = 3.0$, $\xi_n = -1.2$, $T_{ea} = T_{ia} = 0.06$ keV, and $n_{ea} = 5.0 \times 10^{12}$ cm^{-3}. In both cases, $(b - a)/a$ was taken to be 8 percent.

References

[1] N.J. Fisch, Phys. Rev. Lett. **41**, 873 (1978)

[2] C.F.F. Karney, N.J. Fisch, Phys. Fluids **22**, 1817 (1979).

[3] V. Fuchs, R.A. Cairns, M.M. Shoucri, K. Hizanidis, A. Bers, Phys. Fluids **28**, 3619 (1985).

[4] K. Uehara, J. Phys. Soc. Jpn. **53**, 2018 (1984).

[5] K. Uehara, O. Naito, M. Seki, K. Hoshino, Phys. Rev. Lett. **64**, 757 (1990).

[6] X. Meng-Fen, W. Wei-Min, Plasma. Phys. and Contr. Fusion **29**, 621 (1987).

[7] T.M. Antonsen, Jr., and K. Yoshioka, Phys. Fluids **29**, 2235 (1986).

[8] S. Bernabei, C. Daughney, P. Efthimion, W. Hooke, J. Stevens, S. von Goeler, R. Wilson, Phys. Rev. Lett. **49**, 1255 (1982).

[9] M. Porkolab, J.J. Schuss, B. Lloyd, Y. Takase, S. Texter, P.T. Bonoli, C. Fiore, R. Gandy, D. Gwinn, B. Lipschultz, E. Marmar, D. Pappas, R. Parker, P. Pribyl, Phys. Rev. Lett. **53**, 450 (1984).

[10] Y. Ikeda, T. Imai, K. Ushigusa, M. Seki, K. Konishi, O. Naito, M. Honda, K. Kiyono, S. Maebara, T. Nagashima, M. Sawahata, K. Suganuma, N. Suzuki, K. Uehara, K. Yokokura, and the JT-60 Team, Nucl. Fusion **29**, 1815 (1989).

[11] V.E. Golant, Sov. Phys. Tech. Phys. **16** 1980 (1972).

[12] P.L. Colestock and J.L. Kulp, IEEE Trans. Plasma Sci. PS-8, 71 (1980).

[13] P.T. Bonoli, R.C. Englade, Phys. Fluids **29**, 2937 (1986).

[14] K. Yoshioka, T.M. Antonsen, Jr., Nucl. Fusion **26**, 839, (1986).

[15] G. Giruzzi, Nucl. Fusion **27**, 1934 (1987).

[16] V.D. Shafranov, in *Reviews of Plasma Physics*, edited by M.A. Leontovich (Consultants Bureau, New York, 1966), Vol. 2, p. 103.

[17] V.B. Krapchev, D.W. Hewett, A. Bers, Phys. Fluids **28**, 522 (1985).

[18] J.M. Rax, D. Moreau, Nucl. Fusion **29**, 1751 (1989)

[19] S.C. Luckhardt, Nucl. Fusion **27**, 1914 (1987).

[20] T.H. Dupree, Phys. Fluids **9**, 1773 (1966).

[21] The ratio of the autocorrelation time to the trapping time is $\tau_{ac}/\tau_{tr} = w/(u_2 - u_1)$, where $w = [D_{uu}(u_1 + u_2)/6\omega]^{1/3}$.

[22] H.E. Mynick, J.D.Strachan, Phys. Fluids **24**, 695 (1981).

[23] R. Kirkwood, I.H. Hutchinson, S.C. Luckhardt, M. Porkolab, J.P. Squire, Phys. Fluids B **2**, 1421 (1990).

[24] D. Moreau, J.M. Rax, A. Samain, Plasma Phys. and Contr. Fusion **31**, 1895 (1989).

[25] D. Moreau, Y. Peysson, J.M. Rax, A. Samain, J.C. Dumas, Nucl. Fusion **30**, 97 (1990).

[26] M. Shoucri, V. Fuchs, A. Bers, Comput. Phys. Commun. **46**, 337 (1987).

[27] R.G. Littlejohn, J. Plasma Phys. **29**, 111 (1983).

[28] S.C. Chiu, Plasma Phys. and Contr. Fusion **27**, 1525 (1985).

Figure Captions

Figure 1: Model results for Alcator C; (a) normalized diffusion coefficient and (b) electron tail distribution function on a given flux surface, $\rho/a = .16$.

Figure 2: Model results for Alcator C; radial profiles of (a) absorbed power density, S_{rf} (W/cm^3) and (b) RF driven current density, J_{rf} (kA/cm^2).

Figure 3: Model results for Alcator C; radial convection velocity V_ρ (m/sec) as a function of u/v_e at two flux surfaces in the plasma (a) $\rho/a = .16$ and (b) $\rho/a = .32$. The dotted curve shows the prediction of (47) with $\langle n_{\|o} \rangle = 2.0$.

Figure 4: Model results for Alcator C; (a) radial diffusion coefficient, D_ρ (m^2/sec) and (b) diagonal Fokker-Planck element, $D_{\rho\rho}$ (m^2/sec), as functions of u/v_e at a given flux surface, $\rho/a = .16$.

Figure 5: Model results for Alcator C; radial profiles of (a) average radial convection velocity, $\bar{V}_\rho$ (m/sec) and (b) average radial diffusion coefficient, $\bar{D}_\rho$ (m^2/sec).

Figure 6: Model results for JT60; (a) normalized diffusion coefficient and (b) electron tail distribution function on a given flux surface, $\rho/a = .16$.

Figure 7: Model results for JT60; radial profiles of (a) absorbed power density, S_{rf} (W/cm^3) and (b) RF driven current density, J_{rf} (kA/cm^2).

Figure 8: Model results for JT60; radial convection velocity V_ρ (m/sec) as a function of u/v_e at two flux surfaces in the plasma (a) $\rho/a = .16$ and (b) $\rho/a = .32$. The dotted curve shows the prediction of (47) with $\langle n_{\|o} \rangle = 1.75$.

Figure 9: Model results for JT60; (a) radial diffusion coefficient, D_ρ (m^2/sec) and (b) diagonal Fokker-Planck element, $D_{\rho\rho}$ (m^2/sec), as functions of u/v_e at a given flux surface, $\rho/a = .16$.

Figure 10: Model results for JT60; radial profiles of (a) average radial convection velocity, $\bar{V}_\rho$ (m/sec) and (b) average radial diffusion coefficient, $\bar{D}_\rho$ (m^2/sec).

Figure 11: (a) Approximation to D_ρ (m^2/sec) determined from (52) with $\sigma = .15$ and D_{uu} from the JT60 model results. (b) D_ρ (m^2/sec) obtained directly from the model results, same as Figure 9(a).

Figure 12: Model results for JT60; (a) normalized diffusion coefficient and (b) electron tail distribution function at a flux surface further from the center, $\rho/a = .49$.

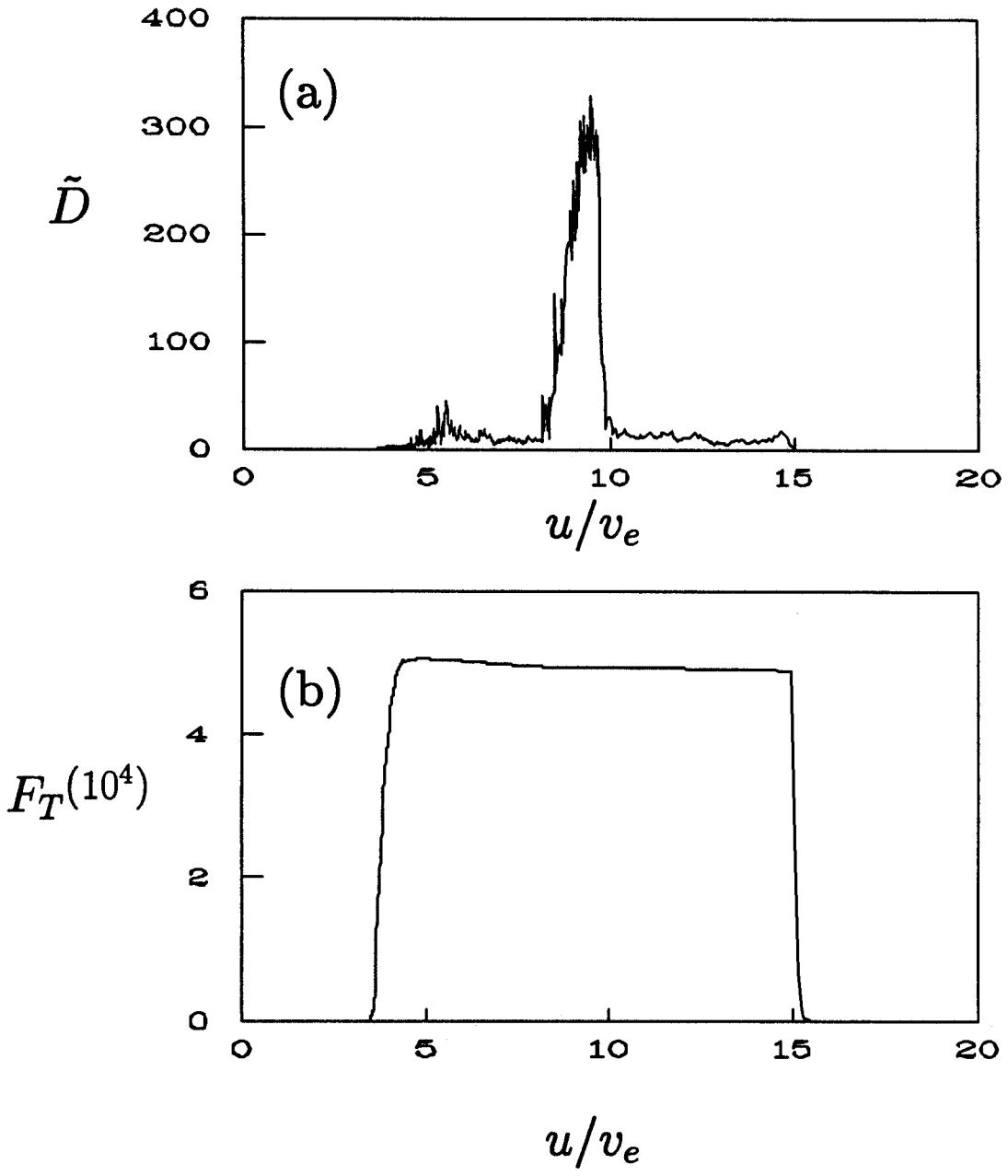

Figure 1: Model results for Alcator C; (a) normalized diffusion coefficient and (b) electron tail distribution function on a given flux surface, $\rho/a = .16$.

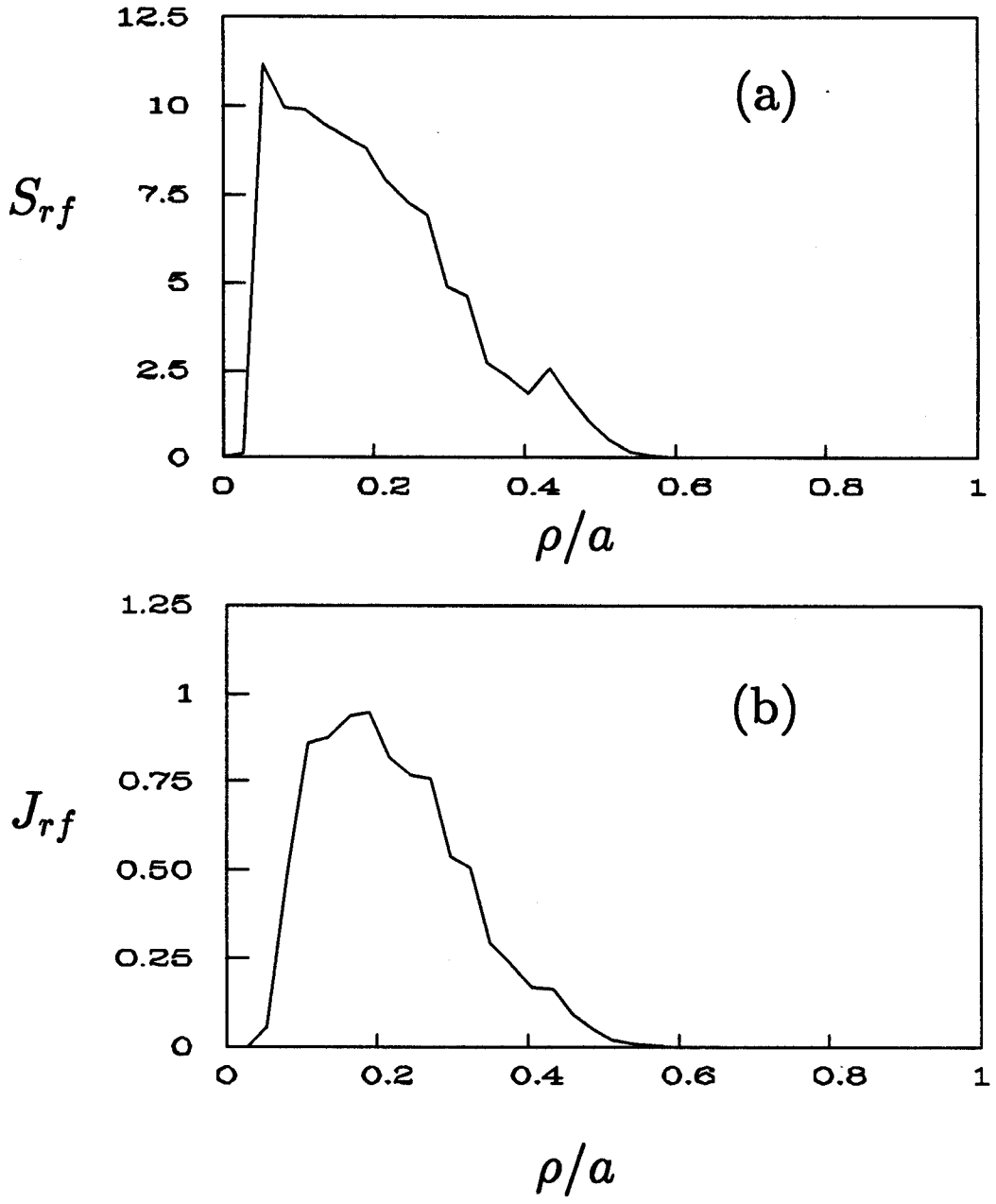

Figure 2: Model results for Alcator C; radial profiles of (a) absorbed power density, S_{rf} (W/cm^3) and (b) RF driven current density, J_{rf} (kA/cm^2).

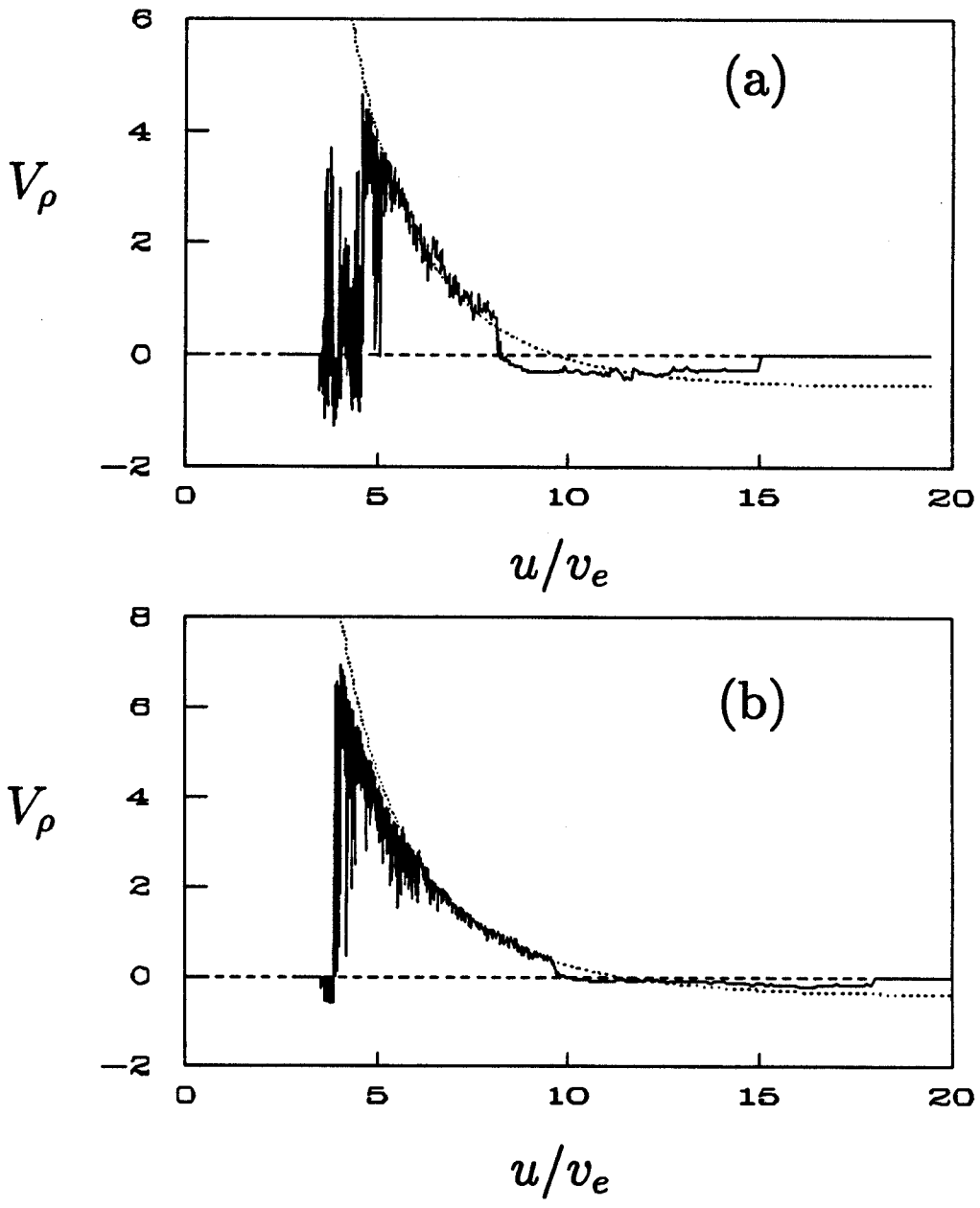

Figure 3: Model results for Alcator C; radial convection velocity V_ρ (m/sec) as a function of u/v_e at two flux surfaces in the plasma (a) $\rho/a = .16$ and (b) $\rho/a = .32$. The dotted curve shows the prediction of (47) with $\langle n_{\|o} \rangle = 2.0$.

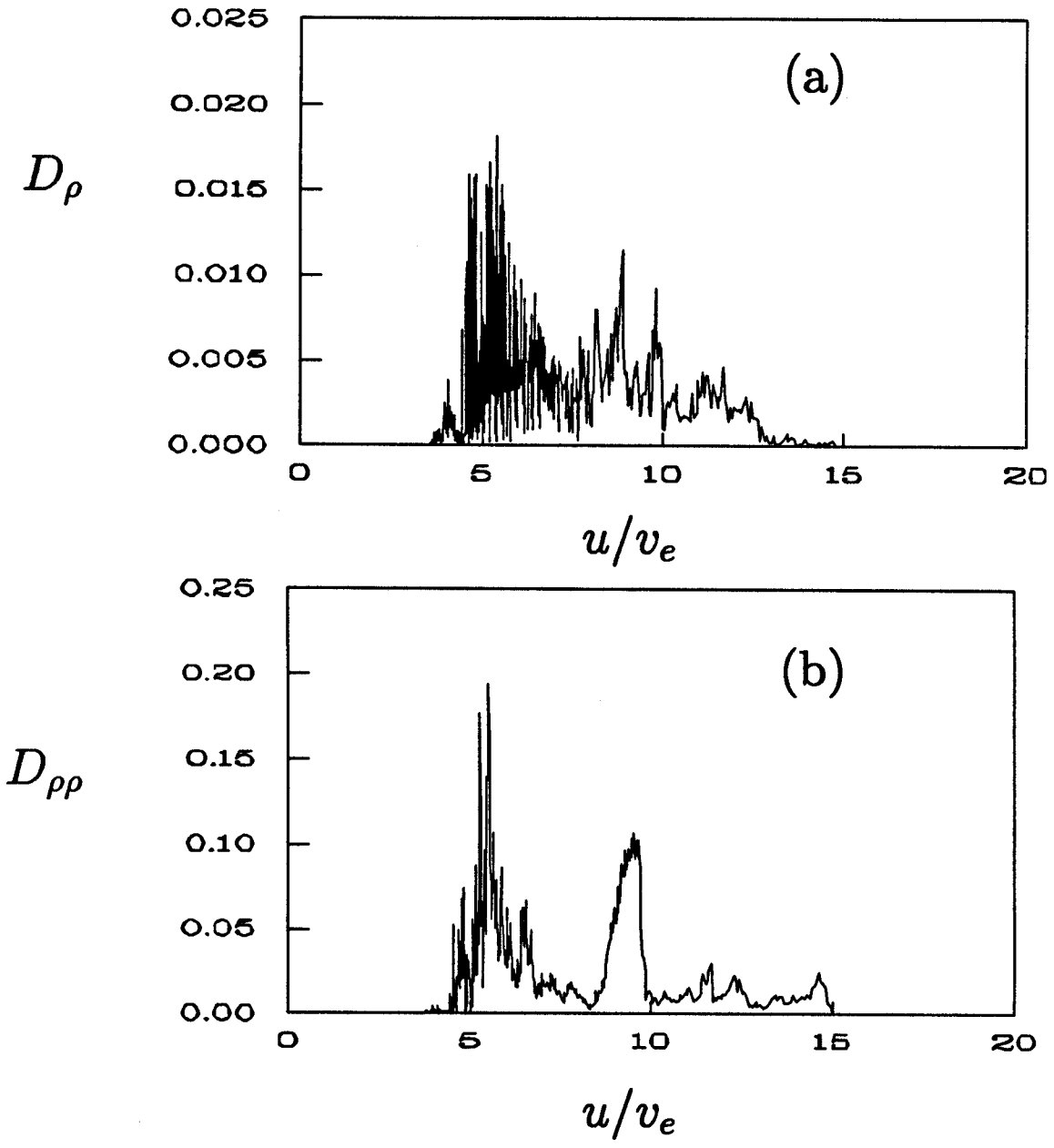

Figure 4: Model results for Alcator C; (a) radial diffusion coefficient, D_ρ (m^2/sec) and (b) diagonal Fokker-Planck element, $D_{\rho\rho}$ (m^2/sec), as functions of u/v_e at a given flux surface, $\rho/a = .16$.

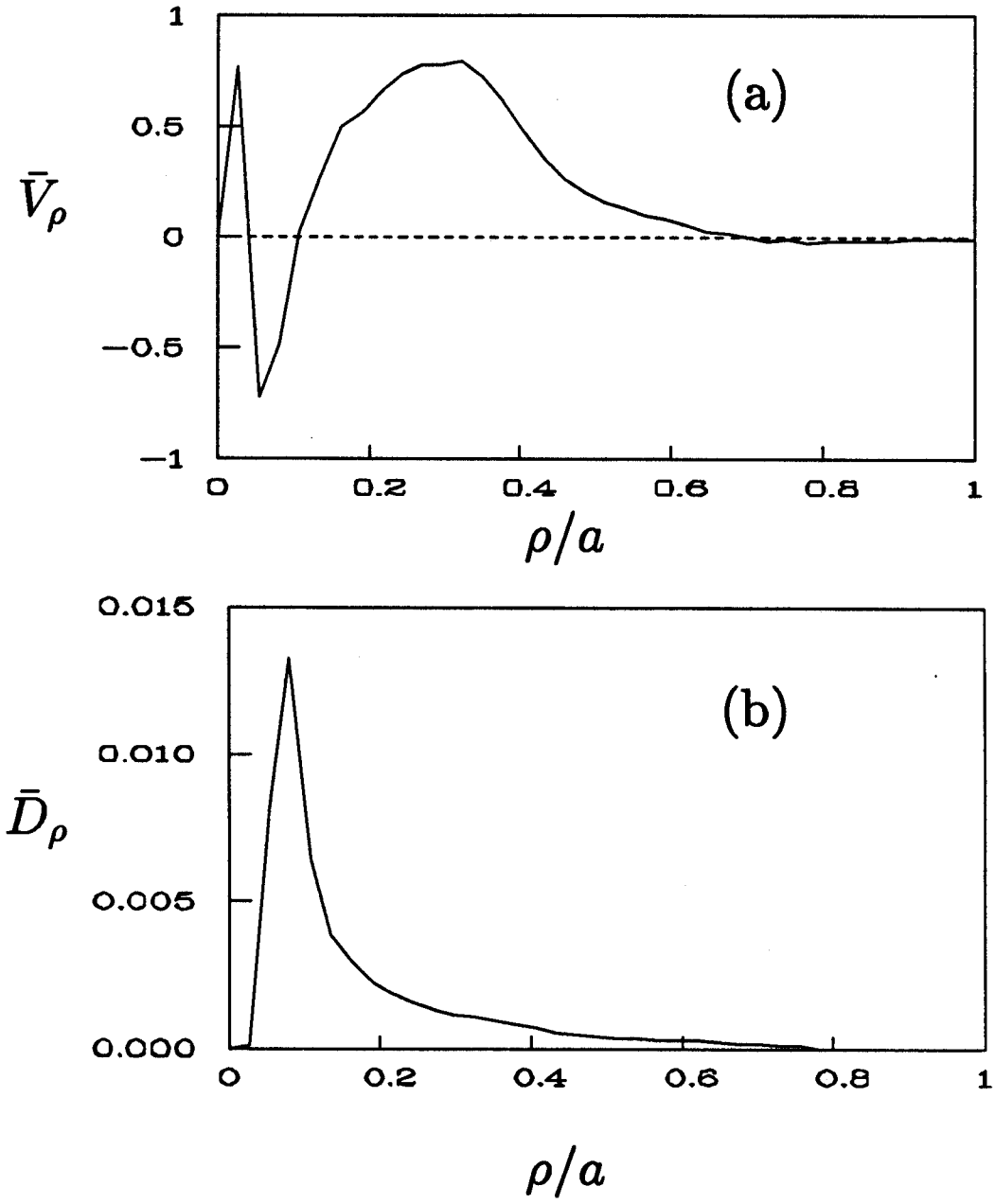

Figure 5: Model results for Alcator C; radial profiles of (a) average radial convection velocity, $\bar{V}_\rho$ (m/sec) and (b) average radial diffusion coefficient, $\bar{D}_\rho$ (m^2/sec).

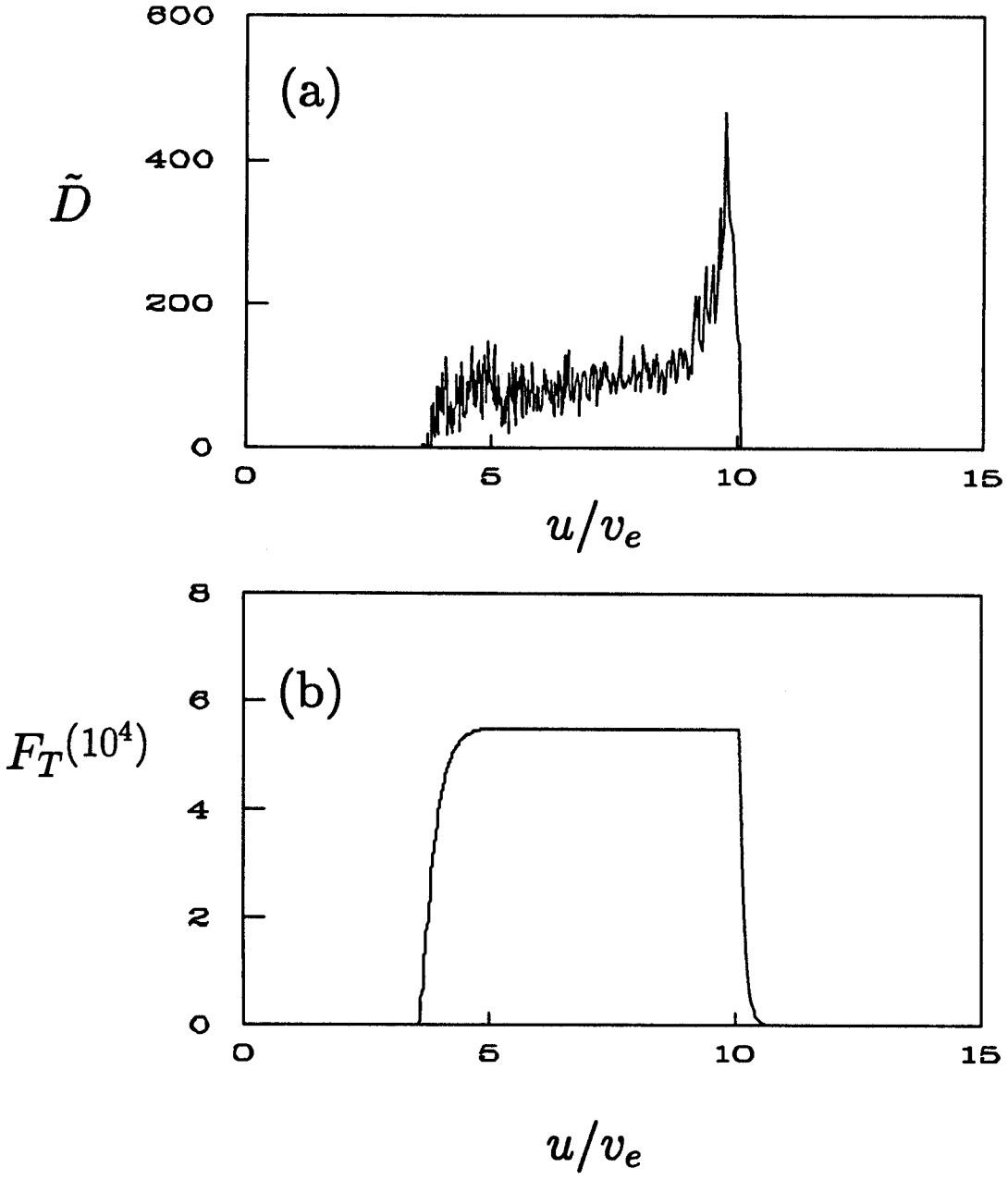

Figure 6: Model results for JT60; (a) normalized diffusion coefficient and (b) electron tail distribution function on a given flux surface, $\rho/a = .16$.

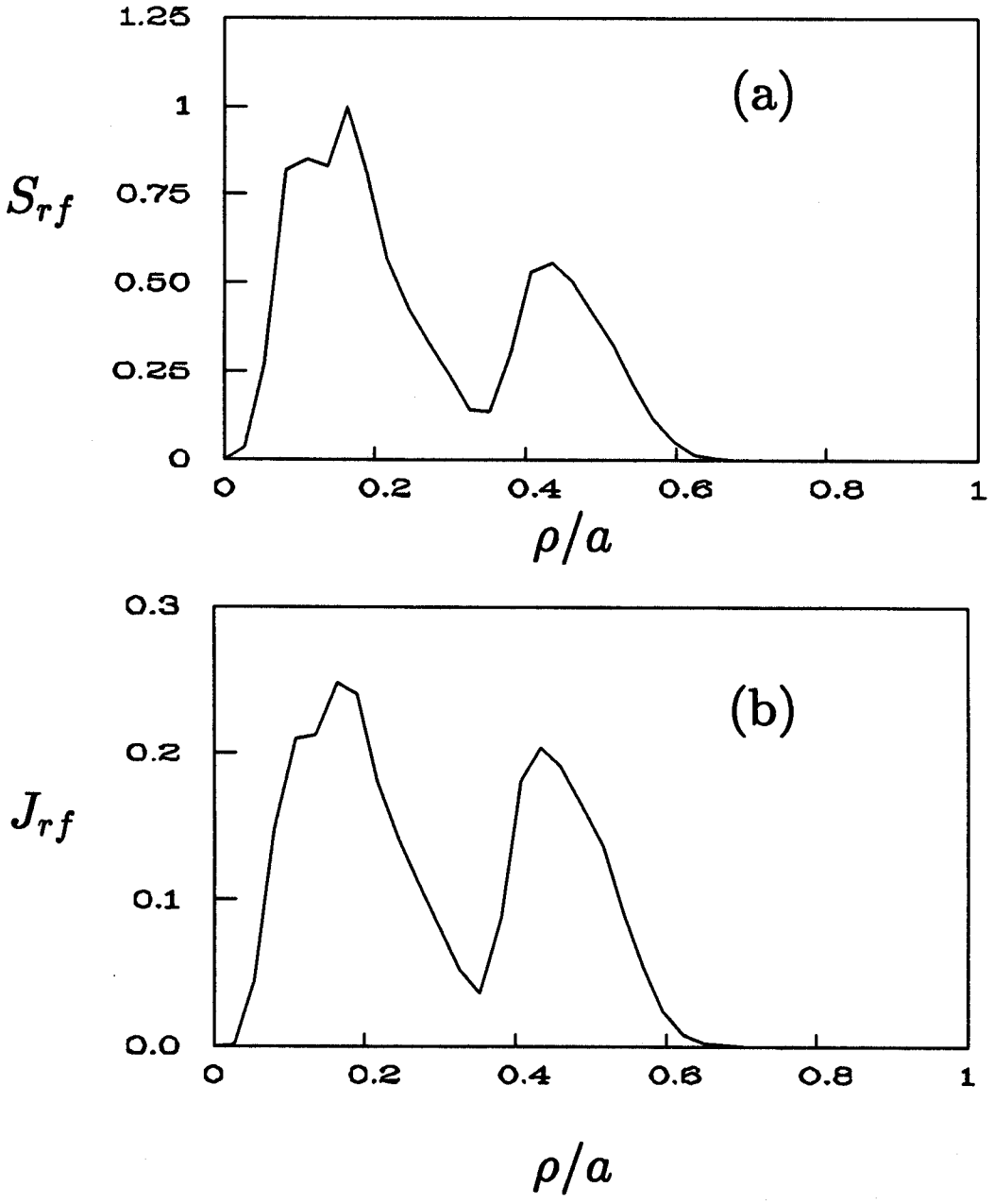

Figure 7: Model results for JT60; radial profiles of (a) absorbed power density, S_{rf} (W/cm^3) and (b) RF driven current density, J_{rf} (kA/cm^2).

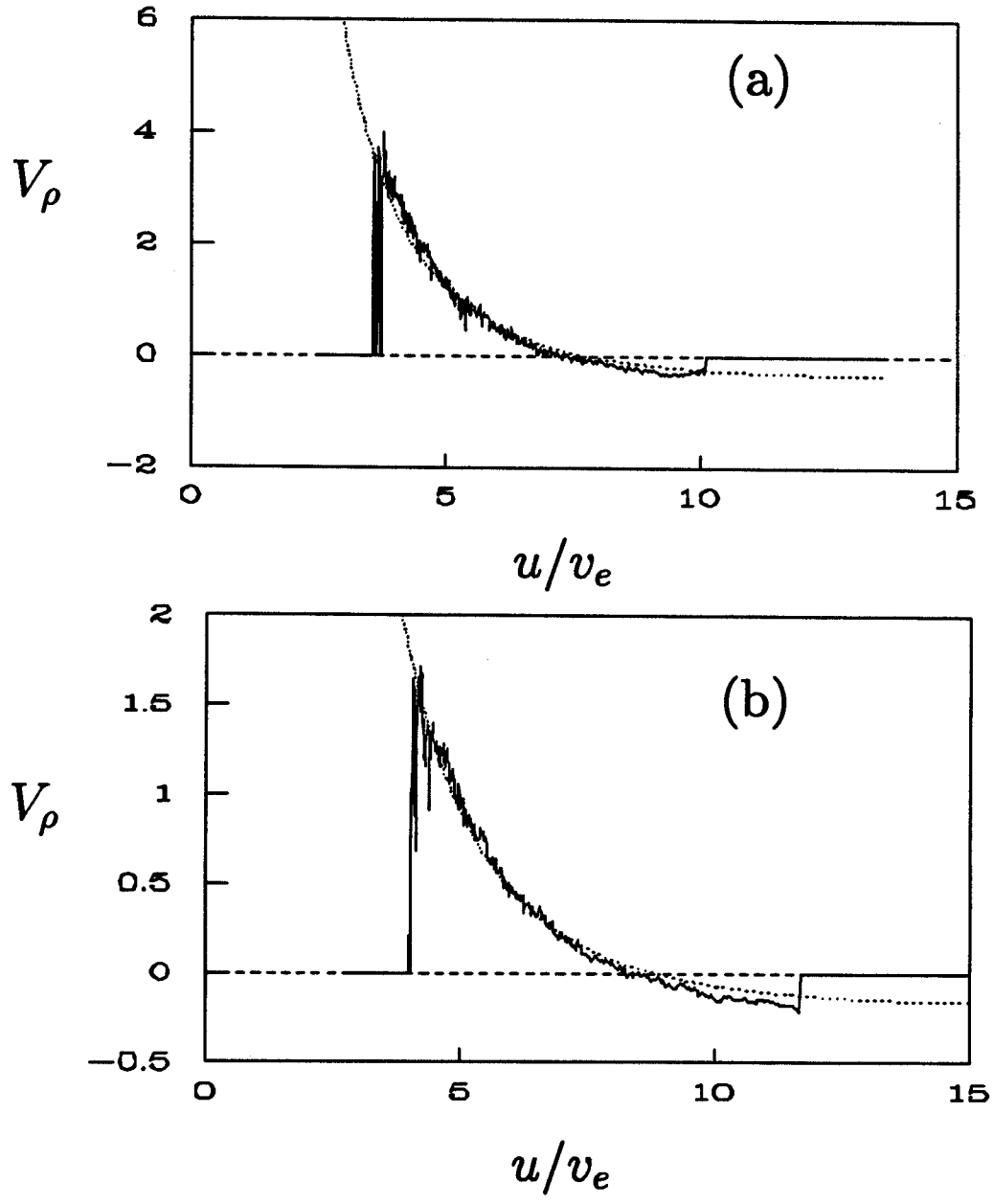

Figure 8: Model results for JT60; radial convection velocity V_ρ (m/sec) as a function of u/v_e at two flux surfaces in the plasma (a) $\rho/a = .16$ and (b) $\rho/a = .32$. The dotted curve shows the prediction of (47) with $\langle n_{\|o} \rangle = 1.75$.

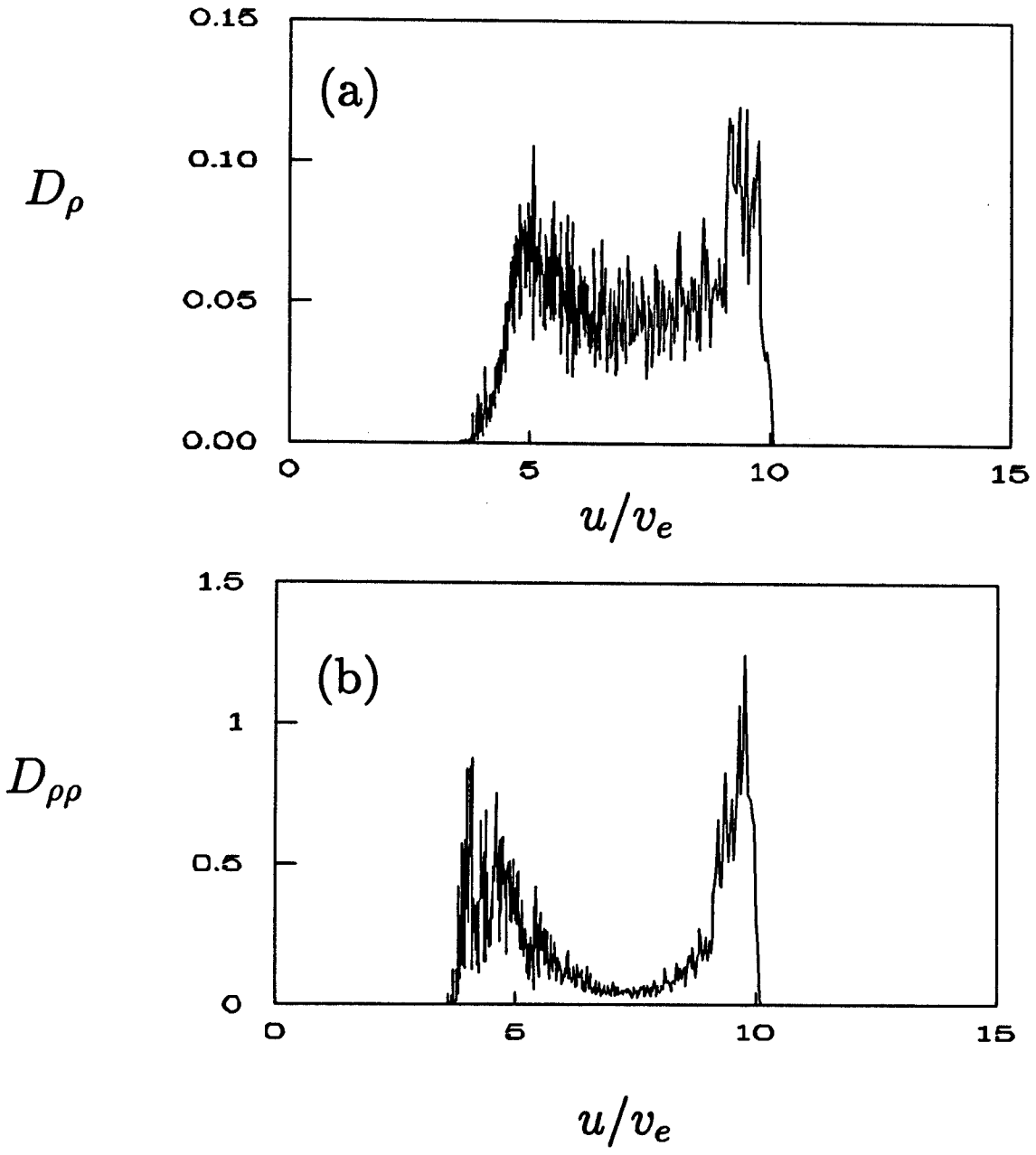

Figure 9: Model results for JT60; (a) radial diffusion coefficient, D_ρ (m^2/sec) and (b) diagonal Fokker-Planck element, $D_{\rho\rho}$ (m^2/sec), as functions of u/v_e at a given flux surface, $\rho/a = .16$.

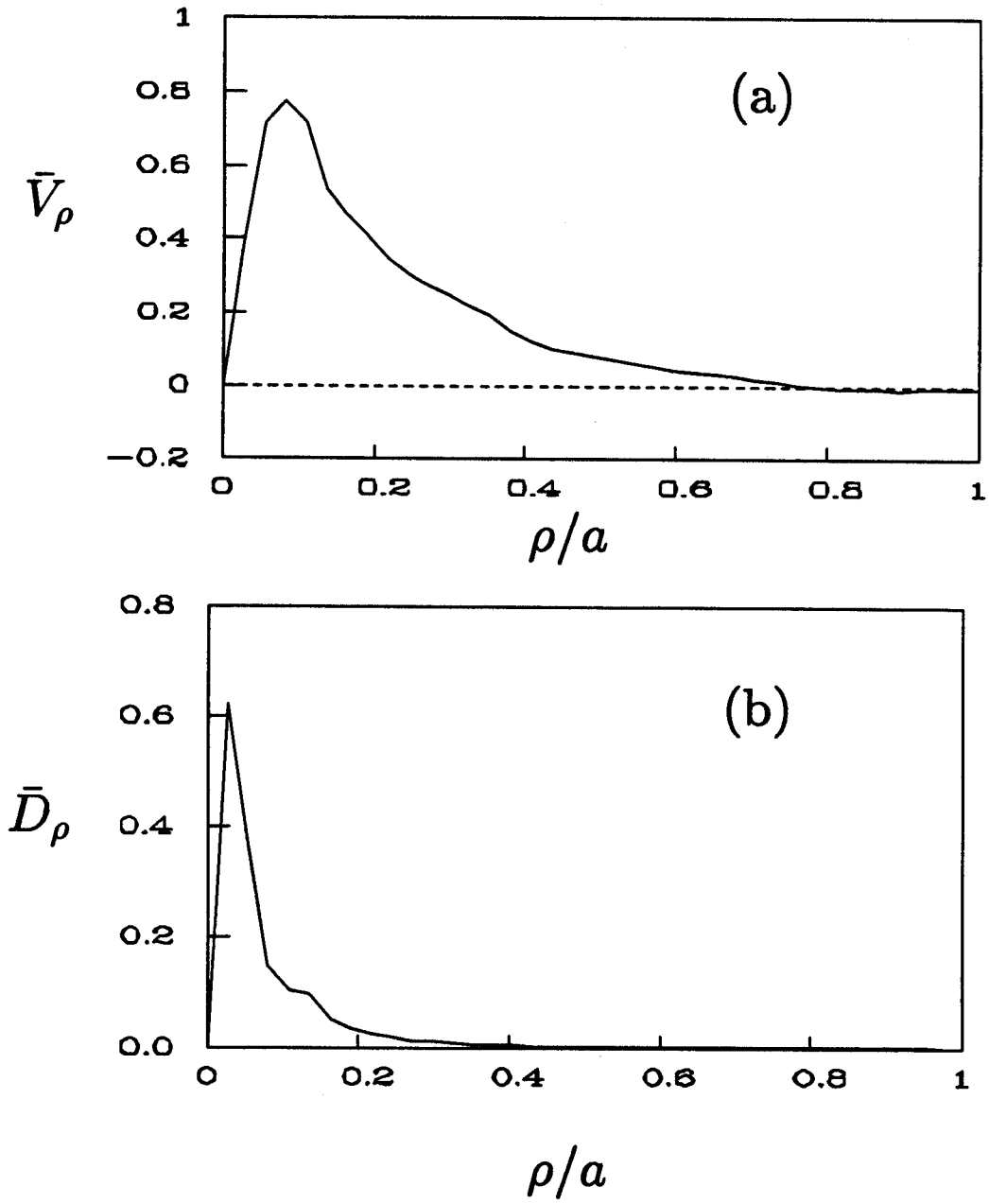

Figure 10: Model results for JT60; radial profiles of (a) average radial convection velocity, $\bar{V}_\rho$ (m/sec) and (b) average radial diffusion coefficient, $\bar{D}_\rho$ (m^2/sec).

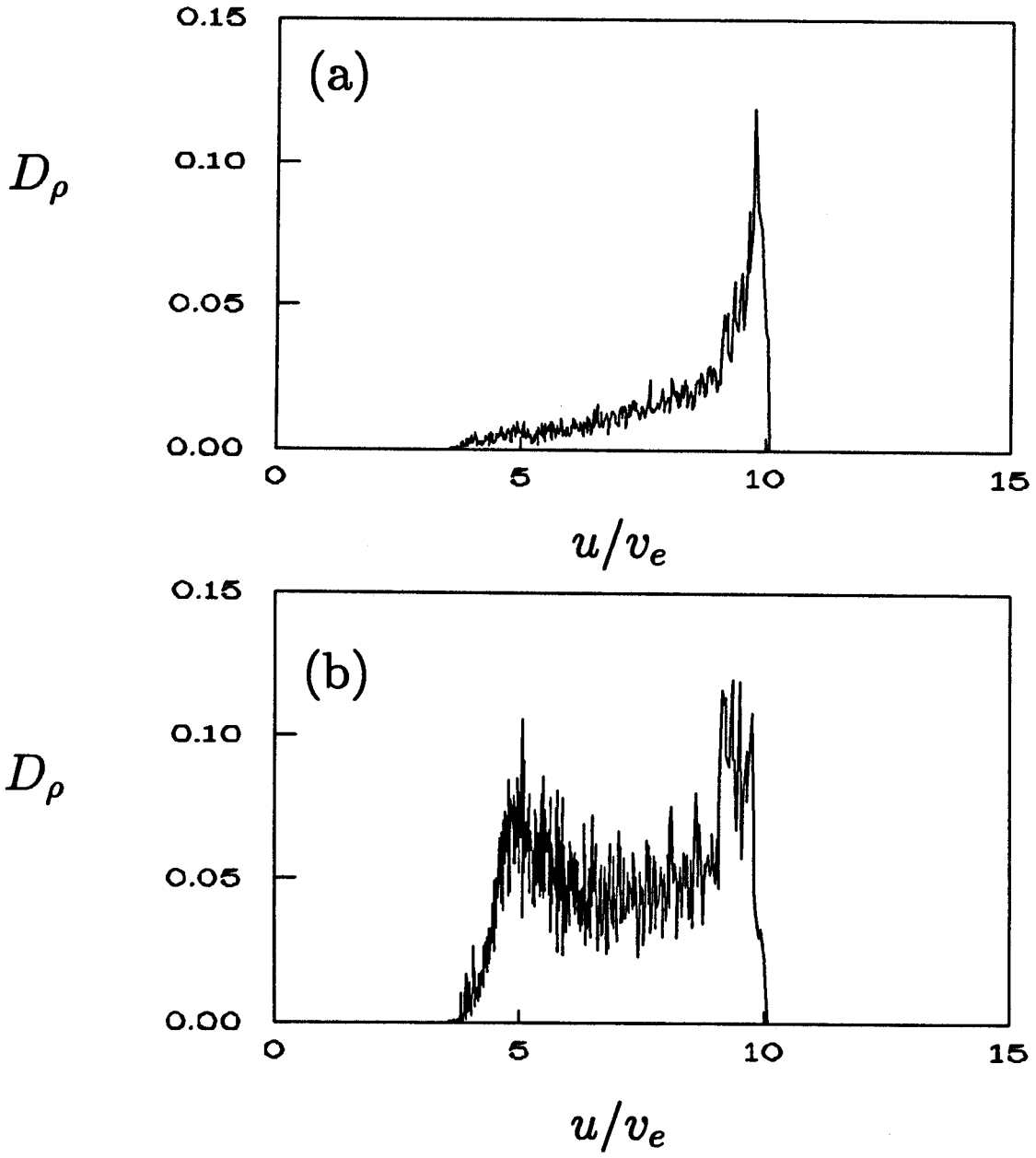

Figure 11: (a) Approximation to D_ρ (m^2/sec) determined from (52) with $\sigma = .15$ and D_{uu} from the JT60 model results. (b) D_ρ (m^2/sec) obtained directly from the model results, same as Figure 9(a).

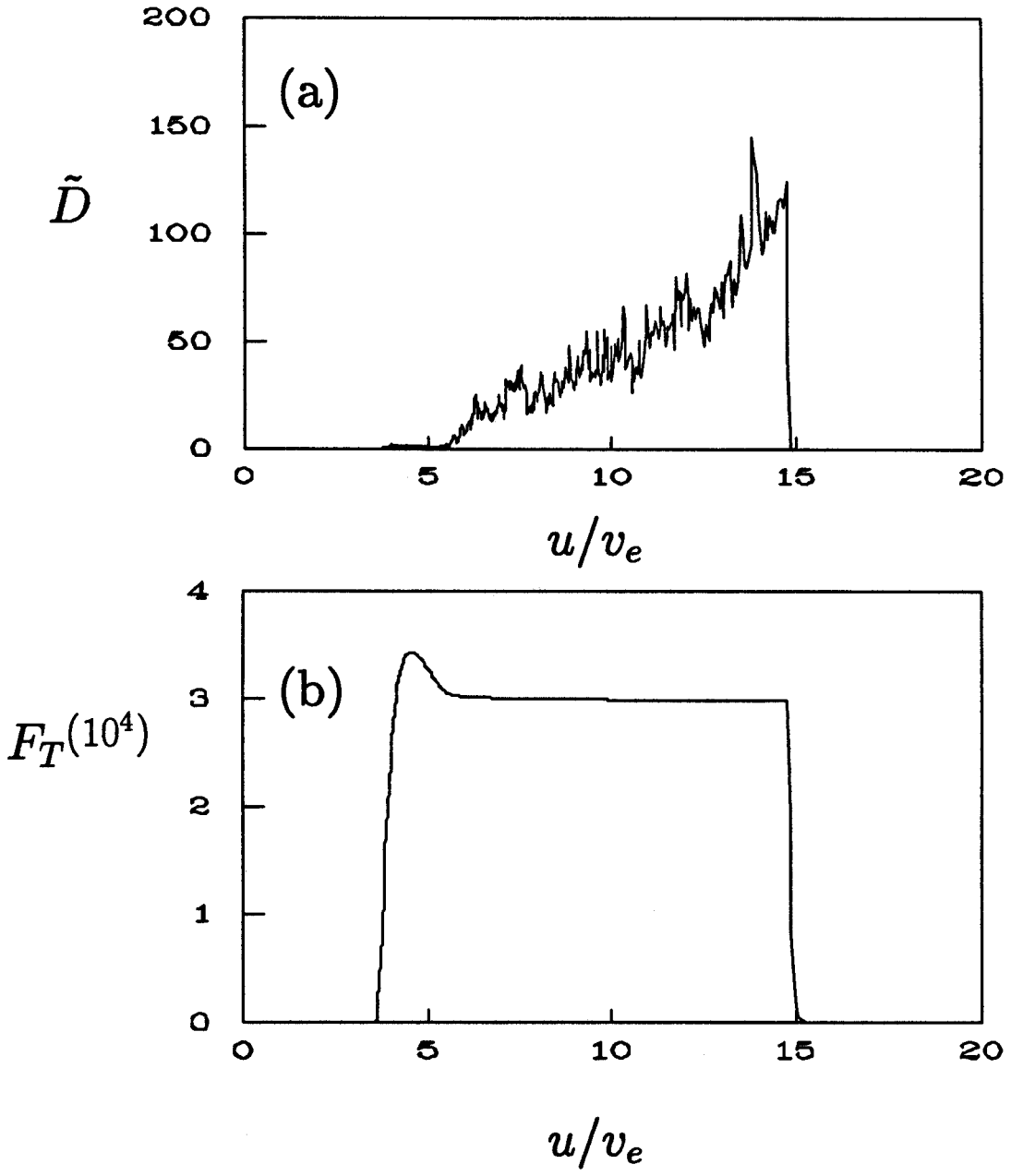

Figure 12: Model results for JT60; (a) normalized diffusion coefficient and (b) electron tail distribution function at a flux surface further from the center, $\rho/a = .49$.